

Novel Collective Excitations and the Quasi-Particle Picture of Quarks Coupled with a Massive Boson at Finite Temperature

Masakiyo KITAZAWA,^{1,2,*} Teiji KUNIHIRO^{1,**} and Yukio NEMOTO^{3,***})

¹*Yukawa Institute for Theoretical Physics, Kyoto University, Kyoto
606-8502, Japan*

²*RIKEN-BNL Research Center, Brookhaven National Laboratory, Upton,
NY 11973, USA*

³*Department of Physics, Nagoya University, Naogya 464-8602, Japan*

*) E-mail: kitazawa@quark.phy.bnl.gov

**) E-mail: kunihiro@yukawa.kyoto-u.ac.jp

***) E-mail: nemoto@hken.phys.nagoya-u.ac.jp

Abstract

Motivated by the observation that there may exist hadronic excitations even in the quark-gluon plasma (QGP) phase, we investigate how the properties of quarks, especially within the quasi-particle picture, are affected by the coupling with bosonic excitations at finite temperature (T), employing Yukawa models with a massive scalar (pseudoscalar) and vector (axial-vector) boson of mass m . The quark spectral function and the quasi-dispersion relations are calculated at one-loop order. We find that there appears a three-peak structure in the quark spectral function with a collective nature when T is comparable with m , irrespective of the type of boson considered. Such a multi-peak structure was first found in a chiral model yielding scalar composite bosons with a decay width. We elucidate the mechanism through which the new quark collective excitations are realized in terms of the Landau damping of a quark (an antiquark) induced by scattering with the thermally excited boson, which gives rise to mixing and hence a level repulsion between a quark (antiquark) and an antiquark-hole (quark-hole) in the thermally excited antiquark (quark) distribution. Our results suggest that the quarks in the QGP phase can be described within an interesting quasi-particle picture with a multi-peak spectral function. Because the models employed here are rather generic, our findings may represent a universal phenomenon for fermions coupled to a massive bosonic excitation with a vanishing or small width. The relevance of these results to other fields of physics, such as neutrino physics, is also briefly discussed. In addition, we describe a new aspect of the plasmino excitation obtained in the hard-thermal loop approximation.

§1. Introduction

The exploration of phase transitions in quantum chromodynamics (QCD) and the examination of the nature of the recently discovered form of QCD matter under extreme conditions, such as high temperature (T) and density, are of great interest. One of the central issues in this field is revealing the physical content of the so-called quark-gluon plasma (QGP) phase. Although it was widely believed for a long time that the QGP phase, even just after the deconfinement transition, is composed of weakly interacting quarks and gluons, in accordance with the asymptotic freedom of QCD, such a view is now believed to be too naive. In fact, it has been being elucidated experimentally and theoretically that the QGP phase near the critical point of the chiral and deconfinement phase transitions has a non-trivial structure, because the strong coupling nature of QCD plays a significant role. Experiments performed at the Relativistic Heavy Ion Collider (RHIC) at BNL are able to probe the QGP phase near the critical temperature (T_c) of the deconfinement and the chiral phase transitions. It has been argued¹⁾ that the experimental results at RHIC suggest that the created matter behaves like a perfect fluid, which implies that the QGP near T_c is a strongly coupled system, and for this reason, it has been called sQGP, where the “s” stands for “strongly coupled”. This suggestion seems to be consistent with the results of recent lattice QCD simulations²⁾ showing that the charmonium states survive at higher temperature above T_c of the deconfinement transition than originally believed.³⁾ The existence of hadronic excitations in the light quark sector in the QGP phase has also been suggested, on the basis of the symmetry nature of the chiral transition,^{4),*)} where it was argued and demonstrated using a chiral effective model that if the chiral transition is second order or nearly second order, there may exist soft modes of the phase transition above T_c that have the same quantum numbers as the sigma meson and the pion.

Quarks and gluons are the basic degrees of freedom in the QGP phase, and therefore it is fundamentally important to clarify their properties even apart from possible hadronic excitations. In fact, the success of the recombination (or coalescence) model⁶⁾ in accounting for the quark-number scaling of the so-called v_2 parameter of the collective flow seen in RHIC experiments strongly suggests that there exist quasi-particles with quark quantum numbers in the matter created at RHIC. Therefore it is imperative^{7),8)} to clarify how the strong coupling nature of the sQGP and the quark quasi-particle picture can be compatible. The present work is concerned with the properties of quarks in a strong coupling system at finite T .

*) See also Ref. 5), in which quite different reasoning is given for the possibility of the color-singlet excitations in the QGP phase.

It is noteworthy that even in the high- T limit, where the hard thermal loop (HTL) approximation⁹⁾ has been established, quarks have some collective nature,¹⁰⁾ as gluons become plasmons:^{11),12)} The quarks have two branches of spectra, i.e., those of the normal quasi-quark and the plasmino,¹³⁾ the latter of which does not exist at zero T and density. The origin of the plasmino excitation at high T is discussed in Ref. 14),^{*)} where it is shown that the appearance of the plasmino at high T is due to the fact that hole states of thermally excited particles and anti-particles can be created.

In the vicinity of T_c of the chiral phase transition, non-perturbative effects are important, and one may expect, on general grounds, that the quarks will possess novel and complicated properties.^{7),16)} In a previous work,⁷⁾ the present authors explored the quark spectrum near but above T_c of the chiral transition, focusing on the effects of the chiral soft modes.⁴⁾ A surprising finding in that study was that the quasi-quarks and quasi-antiquarks acquire a novel collective nature owing to the coupling of the quarks with the soft modes, and as a result, the quark spectral function comes to have a *three-peak* structure as T approaches T_c .⁷⁾ What causes the three-peak structure in the fermion spectrum? In reality, the soft modes correspond to a pronounced peak in the time-like region with a width in the spectral function in a bosonic channel: The peak position at the momentum \mathbf{p} can be expressed approximately as $\omega \simeq \pm\sqrt{m_\sigma^*(T)^2 + |\mathbf{p}|^2}$ with a T -dependent ‘mass’ $m_\sigma^*(T)$, and as T approaches T_c , $m_\sigma^*(T)$ becomes smaller, together with the width of the peaks. This implies that whenever the multi-peak structure of the quark spectral function appears, the soft modes have the character of a well-defined elementary boson with a mass, which is found to be comparable with T .^{7),**)} Thus it is seen that a smaller width of the bosonic excitation is favorable for the multi-peak spectral function, and it is feasible that a system composed of a (massless) quark and an elementary massive boson, as described by a Yukawa model, may exhibit the multi-peak structure in the quark spectral function.

In this paper, we quantitatively examine the quark properties at finite T using Yukawa models with a massive boson coupled to a massless quark. We consider two types of bosons, i.e., massive scalar (pseudoscalar) and vector (axial-vector) bosons with a mass m ; note that because the quark is massless, the scalar (vector) and pseudoscalar (axial-vector) give the

^{*)} The origin of a similar spectrum at zero T but high density is discussed in Ref. 15).

^{**)} The bosonic excitation corresponding to a peak of the spectral function in the time-like region with a small width is a propagating mode with a small damping effect. Such a mode is quite different from those in the (color-)super-conducting transition, which are almost diffusive, with their strength concentrated around the Fermi surface.^{17),18)} Through a coupling with the diffusive soft mode, the quark spectrum can form a *two-peak* structure,¹⁹⁾ which causes the pseudogap in the density of states of quarks.^{16),17)} Thus it is seen that the difference between the numbers of peaks in the quark spectral function comes from the difference between the natures of the respective soft modes.

same results in the perturbation theory. We calculate the spectral function and the quasi-dispersion relation of the quark at finite T at one-loop order. We show that a three-peak structure in the quark spectral function is formed when $T \sim m$, irrespective of the boson type. We elucidate the mechanism through which the new quark collective excitations are realized in terms of the Landau damping of a quark (an antiquark) induced by scattering with thermally excited boson, which gives rise to mixing, and hence level repulsion, between the quark (antiquark) and the antiquark-hole (quark-hole) in the thermally excited quark (antiquark) distribution. Such a mechanism of particle mixing is called “resonant scattering”.^{7),19),20)} We shall also show that the high- T , weak-coupling limit of the fermion spectrum approaches that in the HTL approximation, and thereby show that the plasmino excitation obtained in the HTL approximation can be understood as originating from a level repulsion between collective quark and anti-quark excitations.

Our results suggest that the quarks in the QGP phase can be described within an interesting quasi-particle picture with a multi-peak spectral function, since there may exist bosonic excitations in the QGP phase. Furthermore, noting that the models employed here are rather generic, it is natural to conjecture that the appearance of the novel three-peak structure in the fermion spectrum is a universal phenomenon for fermions coupled to a bosonic excitation with a vanishing or small width, irrespective of the type of the bosonic excitation.

This paper is organized as follows. In §2, the spectral function and the (quasi)-dispersion relation of the fermion, which are frequently used in the following sections, are summarized. We emphasize that the quasi-dispersion relations may not describe the physical excitations when the imaginary part of the quark self-energy is large. In §3, we investigate the fermion spectrum in a Yukawa model with a massive scalar boson. We show that a three-peak structure in the fermion spectral function is formed when $T \sim m$. We clarify the mechanism through which the multi-peak structure in the spectral function is realized in terms of the Landau damping and the resonant scattering. The high- T , weak-coupling limit of the fermion spectrum is also discussed. In §4, we examine the fermion spectrum in a Yukawa model with a massive vector boson. We find that the three-peak structure in the fermion spectral function appears for any type of boson. The relevance of the result to QGP physics is briefly discussed. The last section is devoted to a brief summary and concluding remarks. In the appendices, some technical details of the calculations given in the text are presented.

§2. Generalities concerning the quark spectral function

and dispersion relations at finite temperature

In this section, we summarize general features of the spectral function and the quasi-dispersion relations of the Dirac fermion, which we call a ‘quark’, at finite T . Although the contents of this section may be familiar to the reader, this section serves to introduce the notation used in the subsequent sections.

The quark spectral function $\mathcal{A}(\mathbf{p}, \omega)$ is expressed as¹⁷⁾

$$\mathcal{A}(\mathbf{p}, \omega) = -\frac{1}{\pi} \text{Im} G^R(\mathbf{p}, \omega) \equiv -\frac{1}{\pi} \frac{G^R(\mathbf{p}, \omega) - \gamma^0 G^{R\dagger}(\mathbf{p}, \omega) \gamma^0}{2i}, \quad (2.1)$$

where $G^R(\mathbf{p}, \omega)$ is the retarded Green function of the quark,

$$G^R(\mathbf{p}, \omega) = \frac{1}{(\omega + i\eta)\gamma^0 - \mathbf{p} \cdot \boldsymbol{\gamma} + m_f - \Sigma^R(\mathbf{p}, \omega)}, \quad (2.2)$$

with the quark mass m_f and the retarded self-energy $\Sigma^R(\mathbf{p}, \omega)$. The spectral function $\mathcal{A}(\mathbf{p}, \omega)$ has the same matrix structure as the Green function. Owing to the lack of Lorentz invariance at finite T , $\mathcal{A}(\mathbf{p}, \omega)$ generically has the Dirac structure

$$\mathcal{A}(\mathbf{p}, \omega) = \rho_0(\mathbf{p}, \omega)\gamma^0 - \rho_v(\mathbf{p}, \omega)\hat{\mathbf{p}} \cdot \boldsymbol{\gamma} + \rho_s(\mathbf{p}, \omega), \quad (2.3)$$

where $\hat{\mathbf{p}} = \mathbf{p}/|\mathbf{p}|$ and we have assumed rotational and parity invariances. The temporal part, $\rho_0(\mathbf{p}, \omega)$, represents the quark number excitations of the system.

When $m_f = 0$ and $\text{Tr} \Sigma^R = 0$, with Tr denoting the trace over the Dirac index, the system possesses chiral symmetry, and $\rho_s(\mathbf{p}, \omega)$ vanishes. In this case, the self-energy is written as $\Sigma^R = \Sigma_0 \gamma^0 - \Sigma_v \boldsymbol{\gamma} \cdot \hat{\mathbf{p}}$, and the Green function appearing in Eq. (2.2) can be decomposed using the projection operators $\Lambda_{\pm}(\mathbf{p}) = (1 \pm \gamma^0 \hat{\mathbf{p}} \cdot \boldsymbol{\gamma})/2$ as

$$G^R(\mathbf{p}, \omega) = G_+(\mathbf{p}, \omega)\Lambda_+(\mathbf{p})\gamma^0 + G_-(\mathbf{p}, \omega)\Lambda_-(\mathbf{p})\gamma^0, \quad (2.4)$$

with

$$G_{\pm}(\mathbf{p}, \omega) = \frac{1}{2} \text{Tr}[G^R \gamma^0 \Lambda_{\pm}(\mathbf{p})] = \frac{1}{\omega + i\eta \mp |\mathbf{p}| - \Sigma_{\pm}(\mathbf{p}, \omega)}, \quad (2.5)$$

and $\Sigma_{\pm}(\mathbf{p}, \omega) = (1/2) \text{Tr}[\Sigma^R \Lambda_{\pm}(\mathbf{p})\gamma^0] = \Sigma_0 \mp \Sigma_v$. The spectral function $\mathcal{A}(\mathbf{p}, \omega)$ can also be written as

$$\mathcal{A}(\mathbf{p}, \omega) = \rho_+(\mathbf{p}, \omega)\Lambda_+(\mathbf{p})\gamma^0 + \rho_-(\mathbf{p}, \omega)\Lambda_-(\mathbf{p})\gamma^0, \quad (2.6)$$

where

$$\rho_{\pm}(\mathbf{p}, \omega) = -\frac{1}{\pi} \text{Im} G_{\pm} = \rho_0(\mathbf{p}, \omega) \mp \rho_v(\mathbf{p}, \omega) \quad (2.7)$$

represents the spectrum of the quark and the anti-quark excitations. Note that Σ_{\pm} , G_{\pm} and ρ_{\pm} are scalar functions, while Σ^R , G^R and ρ are matrices in the Dirac space. In a non-interacting system, the spectral function of the massless quark is proportional to the delta function: $\rho_{\pm}^{\text{free}}(\mathbf{p}, \omega) = \delta(\omega \mp |\mathbf{p}|)$. At zero density, $\rho_{+}(\mathbf{p}, \omega)$ and $\rho_{-}(\mathbf{p}, \omega)$ have a simple symmetric property owing to charge conjugation invariance,

$$\rho_{+}(\mathbf{p}, \omega) = \rho_{-}(\mathbf{p}, -\omega). \quad (2.8)$$

The poles of $G_{\pm}(\mathbf{p}, \omega)$, $z = z_{\pm}(\mathbf{p})$, represent collective excitations of the quark and the antiquark sectors, respectively. They are obtained by solving the equations

$$z_{\pm}(\mathbf{p}) \mp |\mathbf{p}| - \Sigma_{\pm}(\mathbf{p}, z_{\pm}(\mathbf{p})) = 0 \quad (2.9)$$

in the complex energy plane. The form of the retarded self-energy guarantees that the solutions z_{\pm} lie in the lower-half plane, owing to causality. Equation (2.9) may have several solutions for fixed momentum $|\mathbf{p}|$, and $\rho_{\pm}(\mathbf{p}, \omega)$ may have a multi-peak structure associated with these poles.

For convenience, we also define the quasi-dispersion relations $\omega = \omega_{\pm}(\mathbf{p})$ as the zero of the *real part* of the inverse Green functions:

$$\omega_{\pm}(\mathbf{p}) \mp |\mathbf{p}| = \text{Re}\Sigma_{\pm}(\mathbf{p}, \omega_{\pm}(\mathbf{p})). \quad (2.10)$$

Solving Eq. (2.10) is much easier than solving Eq. (2.9) in the complex plane. The functions $\omega_{\pm}(\mathbf{p})$ are real numbers, and Eq. (2.10) may have several solutions for fixed \mathbf{p} . When the condition $\text{Im}\Sigma_{\pm}(\mathbf{p}, \omega_{\pm}(\mathbf{p})) \ll \omega_{\pm}(\mathbf{p})$ is satisfied, and hence the quasi-particle picture in the Landau sense is valid, the difference between $\text{Re}z_{\pm}$ and ω_{\pm} is small. Then $\omega_{\pm}(\mathbf{p})$ can be regarded as an approximation of the excitation energy of the quasi-particles and can be used to estimate positions of the peaks in ρ_{\pm} .^{*)} We often use the quasi-dispersion relations in this paper.

§3. Quark spectrum in a Yukawa model with a massive scalar (pseudoscalar) boson

In this section, we investigate the spectrum of a massless quark ψ in a Yukawa model with a massive scalar (pseudoscalar) boson ϕ at finite T . A detailed analysis of a *massive quark* coupled with a *massless boson* at vanishing momentum is given in Ref. 21). As we

^{*)} In this sense, when this condition is satisfied, the peaks of the spectral function and the quasi-dispersion relation, which are gauge-dependent in the gauge theories, accurately reflect the position of the gauge-independent poles of the Green function.

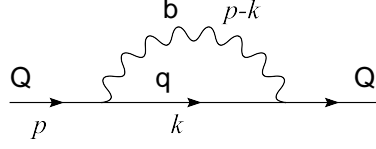


Fig. 1. The quark self-energy at one-loop order.

find below, the finite boson mass gives rise to unexpectedly interesting complications in the quark spectrum, which were not seen in Ref. 21).

We start from the following Lagrangian composed of a quark and a scalar boson:

$$\mathcal{L} = \bar{\psi}(i\cancel{\partial} - g\phi)\psi + \frac{1}{2} (\partial_\mu\phi\partial^\mu\phi - m^2\phi^2). \quad (3.1)$$

Here, g is the coupling constant and m is the boson mass. We note that if the boson is a pseudoscalar, g should be replaced with $i\gamma_5 g$. As we shall see, however, this replacement does not lead to any difference in the results for the quark spectrum.

3.1. Quark self-energy

3.1.1. Formulation

The quark self-energy in the imaginary time formalism at one-loop order, shown in Fig. 1, is given by

$$\tilde{\Sigma}(\mathbf{p}, i\omega_m) = -g^2 T \sum_n \int \frac{d^3\mathbf{k}}{(2\pi)^3} \mathcal{G}_0(\mathbf{k}, i\omega_n) \mathcal{D}(\mathbf{p} - \mathbf{k}, i\omega_m - i\omega_n), \quad (3.2)$$

where $\mathcal{G}_0(\mathbf{k}, i\omega_n) = [i\omega_n\gamma^0 - \mathbf{k} \cdot \boldsymbol{\gamma}]^{-1}$ and $\mathcal{D}(\mathbf{k}, i\nu_n) = [(i\nu_n)^2 - \mathbf{k}^2 - m^2]^{-1}$ are the Matsubara Green functions for the free quark and scalar boson, respectively, and $\omega_n = (2n+1)\pi T$ and $\nu_n = 2n\pi T$ are the Matsubara frequencies for the fermion and boson, respectively.

For the coupling with a pseudoscalar boson, a factor of $i\gamma_5$ appears on both sides of \mathcal{G}_0 in Eq. (3.2). However, these factors cancel out because they anti-commute with \mathcal{G}_0 , and thus the self-energy takes the same form as Eq. (3.2). Therefore, the following results and arguments in this section hold also for coupling with a pseudoscalar boson, as mentioned above.

In accordance with the standard procedure in the imaginary time formalism, we carry out the summation over the Matsubara modes n and the analytic continuation $i\omega_m \rightarrow \omega + i\eta$ (see Appendix A for details). The result is given by

$$\begin{aligned} \Sigma^R(\mathbf{p}, \omega) = g^2 \int \frac{d^3\mathbf{k}}{(2\pi)^3} \frac{1}{2E_b} \left\{ \Lambda_+(\mathbf{k}) \frac{1 + n(E_b) - f(E_f)}{\omega - E_f - E_b + i\eta} + \Lambda_-(\mathbf{k}) \frac{n(E_b) + f(E_f)}{\omega + E_f - E_b + i\eta} \right. \\ \left. + \Lambda_+(\mathbf{k}) \frac{n(E_b) + f(E_f)}{\omega - E_f + E_b + i\eta} + \Lambda_-(\mathbf{k}) \frac{1 + n(E_b) - f(E_f)}{\omega + E_f + E_b + i\eta} \right\} \gamma^0, \quad (3.3) \end{aligned}$$

where $E_f = |\mathbf{k}|$, $E_b = \sqrt{(\mathbf{p} - \mathbf{k})^2 + m^2}$, and $n(E) = [\exp(E/T) - 1]^{-1}$ and $f(E) = [\exp(E/T) + 1]^{-1}$ are the Bose-Einstein and Fermi-Dirac distribution functions, respectively.

The self-energy given in Eq. (3.3) has an ultraviolet divergence, which comes from the T -independent part, $\Sigma^R(\mathbf{p}, \omega)_{T=0} \equiv \lim_{T \rightarrow 0} \Sigma^R(\mathbf{p}, \omega)$. To eliminate this divergence, we renormalize this part by imposing the on-shell renormalization condition. (See Appendix C for details of the renormalization procedure.) The renormalized self-energy is given by

$$\Sigma^R(\mathbf{p}, \omega)_{T=0} = \frac{g^2 \not{p}}{32\pi^2} \left\{ \left(1 - \frac{m^2}{P^2}\right)^2 \ln \frac{P^2 - m^2}{m^2} - \frac{3}{2} + \frac{m^2}{P^2} \right\}, \quad (3.4)$$

with $p_\mu = (\omega, \mathbf{p})$ and $P^2 = p_\mu p^\mu$. Note that there is no infrared divergence in Eq. (3.3) as long as the scalar boson is massive. Since the T -dependent ($T \neq 0$) part, $\Sigma^R(\mathbf{p}, \omega)_{T \neq 0} \equiv \Sigma^R(\mathbf{p}, \omega) - \Sigma^R(\mathbf{p}, \omega)_{T=0}$, has no divergences, we can evaluate it without regularization (see Appendix A). For the numerical calculations of the $T \neq 0$ part, it is convenient to first derive the imaginary part, $\text{Im}\Sigma^R(\mathbf{p}, \omega)_{T \neq 0}$, and then determine the real part using the dispersion (Kramers-Kronig) relation

$$\text{Re}\Sigma^R(\mathbf{p}, \omega)_{T \neq 0} = -\frac{1}{\pi} \text{P} \int_{-\infty}^{\infty} d\omega' \frac{\text{Im}\Sigma^R(\mathbf{p}, \omega')_{T \neq 0}}{\omega - \omega'}, \quad (3.5)$$

where the symbol P denotes the principal value.

The imaginary part of the self-energy, $\text{Im}\Sigma^R(\mathbf{p}, \omega)$, is given by

$$\begin{aligned} \text{Im}\Sigma^R(\mathbf{p}, \omega) = & -\pi g^2 \int \frac{d^3k}{(2\pi)^3} \frac{1}{2E_b} \\ & \times \left\{ \Lambda_+(\mathbf{k})(1+n-f)\delta(\omega - E_f - E_b) \quad \text{(I)} \right. \\ & + \Lambda_-(\mathbf{k})(n+f)\delta(\omega + E_f - E_b) \quad \text{(II)} \\ & + \Lambda_+(\mathbf{k})(n+f)\delta(\omega - E_f + E_b) \quad \text{(III)} \\ & \left. + \Lambda_-(\mathbf{k})(1+n-f)\delta(\omega + E_f + E_b) \right\} \gamma^0 \quad \text{(IV)}, \quad (3.6) \end{aligned}$$

with $f = f(E_f)$ and $n = n(E_b)$. Each term in Eq. (3.6), denoted by (I)-(IV), describes a definite decay process and has support in the region shown in Fig. 2. The details of the physical meaning of each term are discussed in the following.

Let us denote the external quark as Q and the internal quark as q , as shown in Fig. 1. The former is the quasi-quark interacting with scalar bosons, while the latter is a free quark in the approximation used here. The physical meaning of each term in Eq. (3.6) is more transparent when Eq. (3.6) is rewritten in terms of the transition probabilities.²²⁾ We can express Σ_+ defined in §2 as

$$\Sigma_+(\mathbf{p}, \omega) = \bar{u}(p)\Sigma^R(\mathbf{p}, \omega)u(p), \quad (3.7)$$

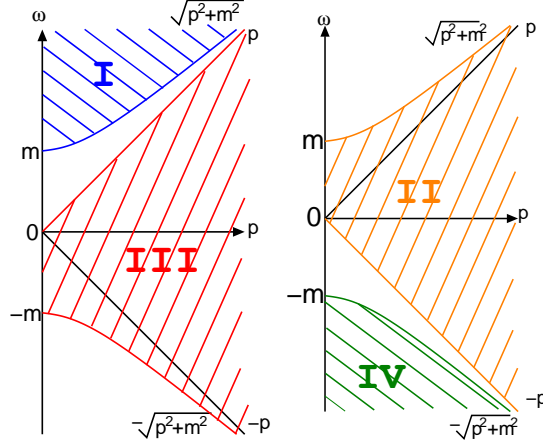


Fig. 2. The supports of the terms (I)-(IV) in Eq. (3.6).

where $u(p)$ is a free quark spinor with the effective mass parameter $\sqrt{P^2}$, which satisfies $(\not{p} - \sqrt{P^2})u(p) = 0$ with the normalization $\bar{u}(p)u(p) = 2\sqrt{P^2}$. Then, we have

$$\begin{aligned}
\text{Im}\Sigma_+(\mathbf{p}, \omega) &= -\frac{1}{2} \int \frac{d^3k_f}{(2\pi)^3} \frac{d^3k_b}{(2\pi)^3} \frac{1}{2E_f 2E_b} \sum_s (2\pi)^4 \\
&\times \left\{ \begin{aligned}
&[\delta^4(p - k_f - k_b)|M(Q \rightarrow q, b)|^2[(1-f)(1-n) + fn] & \text{(I)} \\
&+ [\delta^4(p + k_f - k_b)|M(Q, \bar{q} \rightarrow b)|^2[f(1+n) + n(1-f)] & \text{(II)} \\
&+ [\delta^4(p - k_f + k_b)|M(Q, b \rightarrow q)|^2[n(1-f) + f(1+n)] & \text{(III)} \\
&+ [\delta^4(p + k_f + k_b)|M(Q, \bar{q}, b \rightarrow 0)|^2[fn + (1-f)(1-n)]] & \text{(IV)}, \quad (3.8)
\end{aligned} \right.
\end{aligned}$$

where s is the spin of the quark q and $k_f = (E_f, \mathbf{k})$, $k_b = (E_b, \mathbf{p} - \mathbf{k})$. The amplitudes M are given by

$$\begin{aligned}
M(Q \rightarrow q, b) &= M(Q, b \rightarrow q) = g\bar{u}(p)u(p), \\
M(Q, \bar{q} \rightarrow b) &= M(Q, \bar{q}, b \rightarrow 0) = g\bar{v}(p)u(p), \quad (3.9)
\end{aligned}$$

where $v(p)$ is defined through $(\not{p} + \sqrt{P^2})v(p) = 0$, with the normalization $\bar{v}(p)v(p) = -2\sqrt{P^2}$. The first term in Eq. (3.8) with the statistical factor $(1-f)(1+n)$ describes a decay process $Q \rightarrow q + b$, and that with the factor fn describes the inverse one, $q + b \rightarrow Q$. The second term with the factor $f(1+n)$ describes $Q + \bar{q} \rightarrow b$, and that with the factor $n(1-f)$ describes $b \rightarrow Q + \bar{q}$. The third and the fourth terms are similar. These processes are schematically depicted in Fig. 3. The terms (II) and (III), which involve a thermally excited particle as the incident particle, vanish as $T \rightarrow 0$ and are known as the Landau damping. They play an important role in the structure of the quark spectral function at finite T , as we see below.

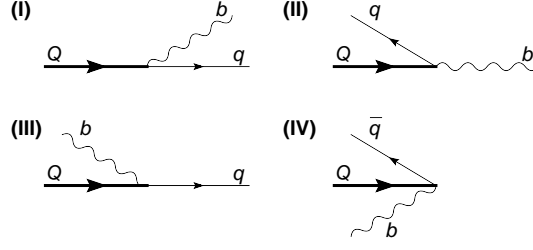


Fig. 3. The kinetic processes contained in $\text{Im}\Sigma_+(\mathbf{p}, \omega)$. (The corresponding inverse ones are not shown.) The thick solid line labeled Q represents the quasi-quark, the thin solid lines labeled q on-shell free quarks, and the wavy lines labeled b the on-shell scalar boson. The incident on-shell particles are thermally excited particles.

Similarly, it can be shown that the quantity $\Sigma_-(\mathbf{p}, \omega) = \bar{v}(p)\Sigma^R(\mathbf{p}, \omega)v(p)$ contains amplitudes for the processes $M(\bar{Q} \rightarrow \bar{q}, b)$, $M(\bar{Q}, q \rightarrow b)$, $M(\bar{Q}, b \rightarrow \bar{q})$, and $M(\bar{Q}, q, b \rightarrow 0)$.

After some manipulations as given in Appendix A, we arrive at the following result

$$\begin{aligned} \text{Im}\Sigma_{\pm}(\mathbf{p}, \omega) = & -\frac{g^2}{32\pi\mathbf{p}^2} \int_{E_f^+}^{E_f^-} dE_f [2|\mathbf{p}|E_f \mp (\mathbf{p}^2 + m^2 - \omega^2 + 2\omega E_f)] \\ & \times [1 + n(\omega - E_f) - f(E_f)] \\ & - \frac{g^2}{32\pi\mathbf{p}^2} [(|\mathbf{p}| \mp \omega)(\pi^2 T^2 \pm \omega^2) \pm \omega m^2] \theta(\mathbf{p}^2 - \omega^2), \end{aligned} \quad (3.10)$$

with $E_f^{\pm} = (\omega^2 - \mathbf{p}^2 - m^2)/2(\omega \pm |\mathbf{p}|)$. For vanishing momentum, we have $\text{Im}\Sigma_+ = \text{Im}\Sigma_-$, and $\text{Im}\Sigma^R$ is simply given by

$$\text{Im}\Sigma^R(\mathbf{p} = 0, \omega) = -\gamma^0 \frac{g^2}{32\pi} \frac{(\omega^2 - m^2)^2}{\omega^3} [n(\omega_b) + f(\omega_q)], \quad (3.11)$$

with

$$\omega_b = \frac{\omega^2 + m^2}{2\omega}, \quad \omega_q = -\frac{\omega^2 - m^2}{2\omega}. \quad (3.12)$$

3.1.2. Numerical results

In the upper panel of Fig. 4, we plot $\text{Im}\Sigma_+(\mathbf{p}, \omega)/g^2$, which is independent of g , for vanishing momentum and several temperatures. We see that $\text{Im}\Sigma_+(\mathbf{0}, \omega)/g^2$ vanishes at $\omega = 0, \pm m$ for all T . These values of ω are located in the boundaries of the regions (I)–(IV) shown in Fig. 2. The vanishing decay rate at $\omega = \pm m$ is due to the suppression of the phase space; energy-momentum conservation requires vanishing momentum of the on-shell (anti)quark for each process at $\omega = \pm m$. Near $\omega = 0$, by contrast, the distribution functions in Eq. (3.11) suppress the decay rate, because the on-shell energies of the boson and the quark, $|\omega_b|$ and $|\omega_q|$, go to infinity as $\omega \rightarrow 0$.

From Fig. 4, we see that $\text{Im}\Sigma_+(\mathbf{p}, \omega)$ takes finite values only for $|\omega|/m > 1$ at $T = 0$; the corresponding decay processes are represented by (I) and (IV) in Fig. 3. At finite T ,

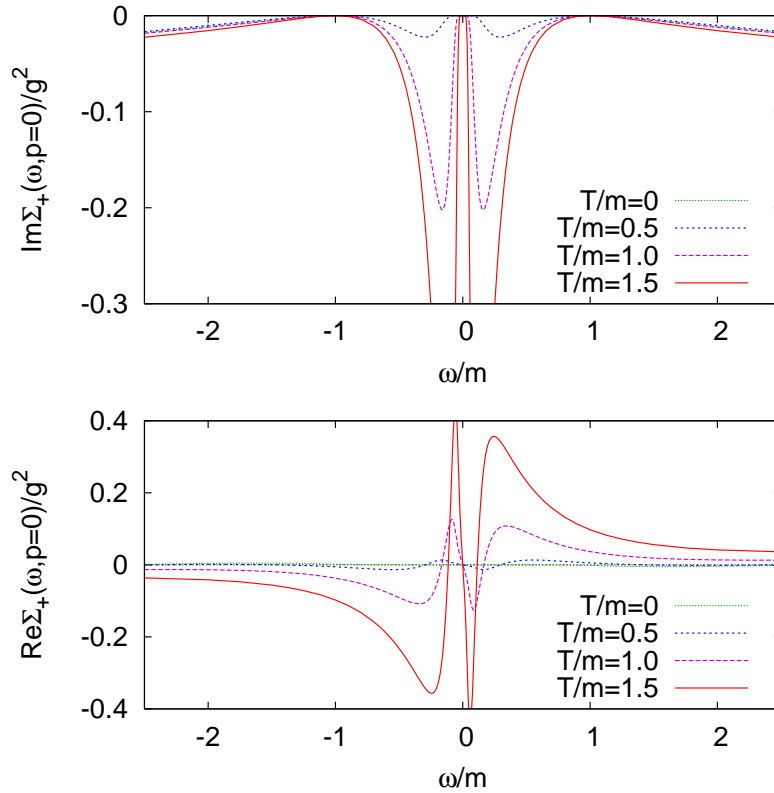


Fig. 4. The imaginary and real parts of the self-energy $\Sigma_+(\mathbf{p}, \omega)$ at zero momentum and several temperatures.

the Landau damping has a significant effect, and $\text{Im}\Sigma_+(\mathbf{p}, \omega)$ has support in the regions (II) and (III) in Fig. 2. The height of the two peaks in these regions increase rapidly as T increases, and for $T \simeq m$, the Landau damping comes to dominate the decay rates, owing to the processes (I) and (IV) in the energy range shown in Fig. 4.

Using the dispersion relation given in Eq. (3.5), we can understand the qualitative behavior of $\text{Re}\Sigma_+(\mathbf{p}, \omega)$ from that of the imaginary part: If there is a sharp peak in the imaginary part, the real part has a step increase at the same energy. In order to see this relation, we plot $\text{Re}\Sigma_+(\mathbf{p}, \omega)/g^2$ for $\mathbf{p} = 0$ in the lower panel of Fig. 4. It is seen that there appears oscillating behavior around $\omega = 0$, and the amplitude of this oscillation grows rapidly as T increases, along with the growth of the peaks in $\text{Im}\Sigma_+(\mathbf{p}, \omega)$.

The other important property of $\Sigma_+(\mathbf{p}, \omega)$ shown in Fig. 4 is that both $\text{Re}\Sigma_+(\mathbf{0}, 0)$ and $\text{Im}\Sigma_+(\mathbf{0}, 0)$ vanish for all T . The fact that $\Sigma^R(\mathbf{0}, 0)$ vanishes implies the existence of a pole of the quark propagator at the origin (see Eq. (2.9)). (The reason that $\text{Im}\Sigma_+(\mathbf{0}, 0)$ vanishes is explained above.) The vanishing of the real part can be easily understood from the dispersion relation and the fact that $\text{Im}\Sigma_+(\mathbf{0}, \omega)$ is an even function of ω . Thus we find

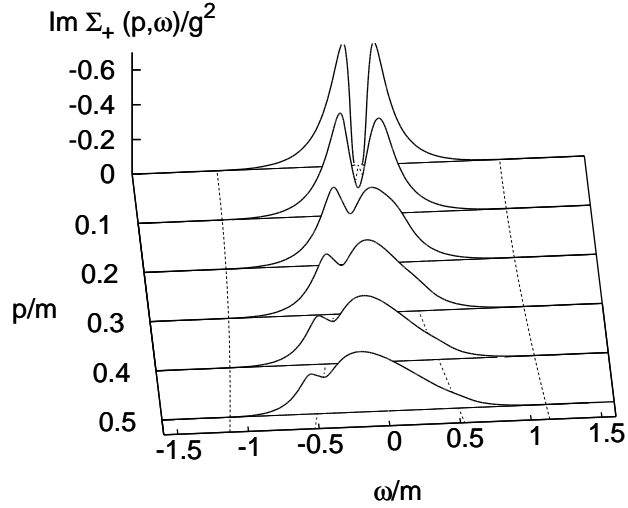


Fig. 5. The imaginary part of the self-energy $|\text{Im}\Sigma_+(\mathbf{p}, \omega)|$ for $T/m = 1.5$. The dashed curves in the ω - \mathbf{p} plane denote $\omega = \pm\sqrt{|\mathbf{p}|^2 + m^2}$ and $\omega = \pm\mathbf{p}$.

that $\text{Re}\Sigma_+(\mathbf{0}, \omega)$ is an odd function of ω .

In Fig. 5, we display $|\text{Im}\Sigma_+(\mathbf{p}, \omega)|/g^2$ at finite momenta and energies for $T/m = 1.5$. The two separated peaks at $\mathbf{p} = \mathbf{0}$, coming from the Landau damping, tend to overlap, and are smeared as \mathbf{p} becomes large.

3.1.3. Asymptotic behavior in the high temperature, weak coupling limit

Finally, let us consider the asymptotic behavior of $\Sigma^R(\mathbf{p}, \omega)$ in the high T , weak coupling limit, i.e. $gT \rightarrow \infty$ and $T/m \rightarrow \infty$, with $g^2T \rightarrow 0$.

In this limit, the leading contribution to the imaginary part, $\text{Im}\Sigma^R(\mathbf{p}, \omega)$, comes from the terms which explicitly include the factor T^2 in Eq. (3.10). Thus, the asymptotic form of $\text{Im}\Sigma^R(\mathbf{p}, \omega)$ is given by

$$\text{Im}\Sigma^R(\mathbf{p}, \omega)|_{T \rightarrow \infty} = -\frac{\pi g^2 T^2}{32} \left(\frac{\gamma^0}{|\mathbf{p}|} - \frac{\omega \hat{\mathbf{p}} \cdot \boldsymbol{\gamma}}{\mathbf{p}^2} \right) \theta(\mathbf{p}^2 - \omega^2). \quad (3.13)$$

The real part in this limit is easily calculated using Eq. (3.13) and the dispersion relation given in Eq. (3.5). We then obtain the following asymptotic form of $\Sigma^R(\mathbf{p}, \omega)$:

$$\Sigma^R(\mathbf{p}, \omega)|_{T \rightarrow \infty} = m_T^2 \frac{\gamma^0}{|\mathbf{p}|} Q(\mathbf{p}, \omega) + m_T^2 \frac{\hat{\mathbf{p}} \cdot \boldsymbol{\gamma}}{|\mathbf{p}|} \left(1 - \frac{\omega}{|\mathbf{p}|} Q(\mathbf{p}, \omega) \right), \quad (3.14)$$

with the thermal mass $m_T = gT/4$ and

$$Q(\mathbf{p}, \omega) = \frac{1}{2} \ln \left| \frac{\omega + |\mathbf{p}|}{\omega - |\mathbf{p}|} \right| - i \frac{\pi}{2} \theta(\mathbf{p}^2 - \omega^2). \quad (3.15)$$

Equation (3.14) is the same as the fermion self-energy of QED and QCD in the HTL approximation,¹⁰⁾ apart from the definition of the thermal mass. Therefore, the quark spectrum in the Yukawa model in the limit $gT \rightarrow \infty$ ($T/m \rightarrow \infty$) with $g \rightarrow 0$ is equivalent to the well-known spectrum in the gauge theories.¹²⁾

We note that the analytic structure of the self-energy is qualitatively different from that at intermediate T , i.e. for $T \simeq m$; there is no pole of the propagator at the origin in this limit, because $\text{Re}\Sigma_+(\mathbf{0}, \omega \rightarrow 0)$ behaves as $\sim 1/\omega$ and hence never vanishes, while $\text{Im}\Sigma_+(\mathbf{0}, \omega \rightarrow 0)$ vanishes. This change in the self-energy is reflected in that of the peak structure of the spectral function, as discussed in the next subsection.

3.2. Quark spectral function at various temperatures

In this subsection, we examine how the quasi-particle picture of the quark changes at finite T by studying the quark spectral function $\rho_{\pm}(\mathbf{p}, \omega)$ and the quasi-dispersion relation $\omega_{\pm}(\mathbf{p})$. We fix the coupling constant as $g = 1$ throughout this subsection to elucidate the T dependence of the spectrum. The g dependence will be discussed in a subsequent subsection. Because the only dimensional parameter in Eq. (3.1) is the boson mass m , we scale all the dimensional parameters T, ω and \mathbf{p} by m .

3.2.1. Quark spectral function at zero temperature and the hard thermal loop approximation

Before presenting the numerical results, we briefly review the quark spectrum at $T = 0$ and high T limit in our model. The analytic form of the quark self-energy at $T = 0$ is given in Eq. (3.4). In this case, the poles of the quark propagator are on the light cone, $\omega = \pm|\mathbf{p}|$, because we have employed the on-shell renormalization condition to derive the self-energy appearing in Eq. (3.4). The quark spectral functions $\rho_{\pm}(\mathbf{p}, \omega)$ are then given by

$$\rho_{\pm}(\mathbf{p}, \omega) = Z(0) \cdot \delta(\omega \mp |\mathbf{p}|) + \rho_{\pm}^{(\text{cont})}(\mathbf{p}, \omega), \quad (3.16)$$

where the T -dependent residue $Z(T)$ is exactly unity at $T = 0$ under the on-shell renormalization condition, and the continuum part $\rho_{\pm}^{(\text{cont})}$ takes finite values for $|\omega| > \sqrt{\mathbf{p}^2 + m^2}$.
*)

In the high T , weak coupling limit, the quark spectrum approaches that calculated in the HTL approximation in the gauge theories with the thermal mass $m_T = gT/4$, as does the quark self-energy (see the previous subsection). In this limit, both $\rho_+(\mathbf{p}, \omega)$ and $\rho_-(\mathbf{p}, \omega)$ have two delta-functions corresponding to the normal quasi-particle and plasmino excitations, in addition to the continuum part in the space-like region^{10), 14)} (see Eqs. (3.14) and (3.15)). In

*) Some readers may be uneasy about the violation of the sum rule for the spectral function, $\int_{-\infty}^{\infty} d\omega \rho_{\pm}(\mathbf{p}, \omega) = 1$. It should be noted here that in relativistic field theory, this sum rule does not necessarily hold after the renormalization.¹⁰⁾

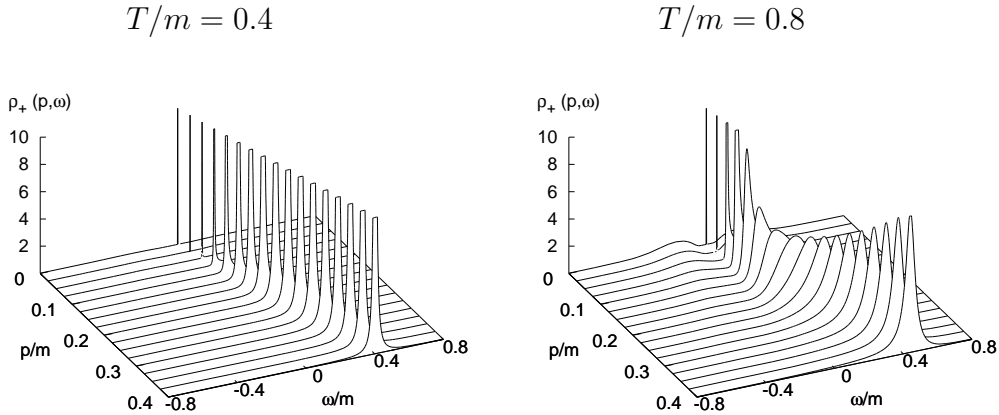


Fig. 6. The quark spectral function $\rho_+(\mathbf{p}, \omega)$ for $T/m = 0.4$ and $T/m = 0.8$.

the high T limit with fixed g , these two peaks have widths of the order of gm_T .¹⁰⁾

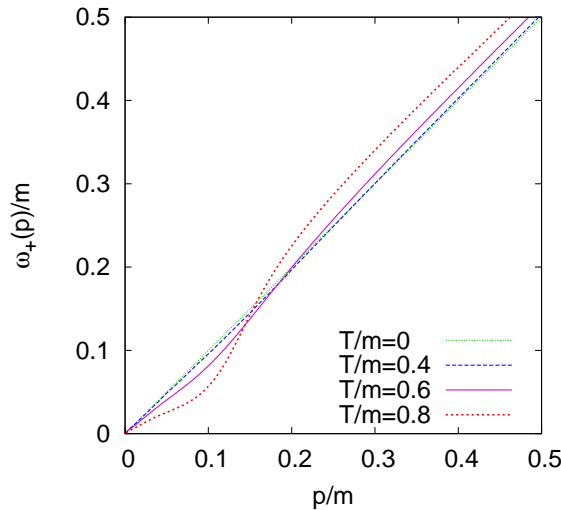


Fig. 7. The quasi-dispersion relation $\omega_+(\mathbf{p})$ for several values of T .

3.2.2. Quark spectral function at low temperature

In Figs. 6 and 7, we plot the spectral function $\rho_+(\mathbf{p}, \omega)$ and the quasi-dispersion relation $\omega_+(\mathbf{p})$ of the quark part for relatively low temperatures, i.e., $T < m$. The anti-quark parts ρ_- and $\omega_-(\mathbf{p})$ can be determined from the symmetric properties given in Eq. (2.8) and the relation $\omega_-(\mathbf{p}) = -\omega_+(\mathbf{p})$. At $T/m = 0.4$, the spectral function $\rho_+(\mathbf{p}, \omega)$ and $\omega_+(\mathbf{p})$ are almost the same as those at $T = 0$; $\rho_+(\mathbf{p}, \omega)$ has sharp quasi-particle peaks around $\omega = |\mathbf{p}|$, and $\omega_+(\mathbf{p}) \simeq |\mathbf{p}|$. At $T/m = 0.8$, the quasi-particle peaks are clearly deformed near $|\mathbf{p}|/m = 0.15$. The quasi-dispersion relation also deviates from the free one near $|\mathbf{p}|/m = 0.15$. We note that this relation exhibits an unphysical acausal behavior; the

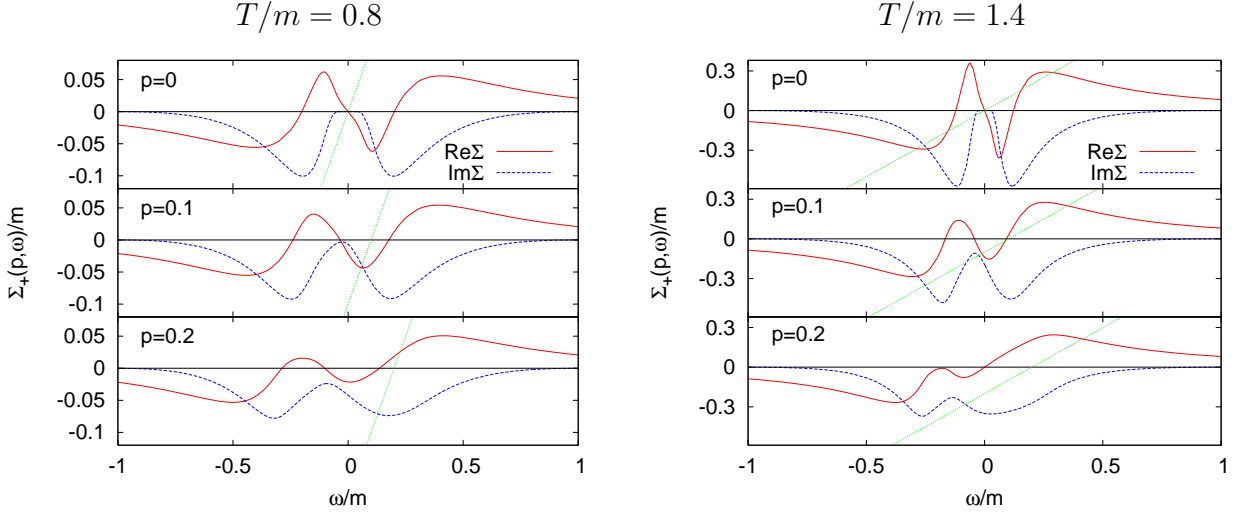


Fig. 8. The quark self-energy $\Sigma_+(\mathbf{p}, \omega)$ for several momenta with $T/m = 0.8$ and 1.4 . The dotted line represents the l.h.s. of Eq. (2.10), i.e., $\omega - |\mathbf{p}|$.

imaginary part of the self-energy is large in this momentum region, as shown in Fig. 8, and thus the quasi-dispersion relation becomes unphysical in this region.

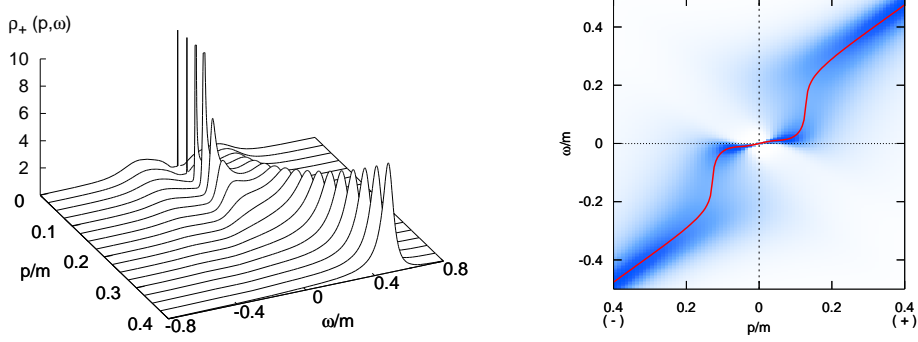
To understand the behavior of $\rho_+(\mathbf{p}, \omega)$ and $\omega_+(\mathbf{p})$ depicted in Figs. 6 and 7, we show the real and imaginary parts of $\Sigma_+(\mathbf{p}, \omega)$ at $T/m = 0.8$ and several momenta in the left panel of Fig. 8. We see that there are two peaks in $\text{Im}\Sigma_+(\mathbf{0}, \omega)$ for positive and negative energies, corresponding to the terms (II) and (III) in Eq. (3.6), respectively. It is seen that $\text{Re}\Sigma_+(\mathbf{p}, \omega)$ exhibits a steep rise in the two regions corresponding to these peaks. We also plot the lines $\omega - |\mathbf{p}|$, i.e. the l.h.s. of Eq. (2.10), by the dotted lines in Fig. 8. Since the quasi-dispersion $\omega_+(\mathbf{p})$ is given by Eq. (2.10), $\omega_+(\mathbf{p})$ corresponds to the points of intersection of the dotted lines and $\text{Re}\Sigma_+(\mathbf{p}, \omega)$. We see that the crossing points depend strongly on the shape of $\text{Re}\Sigma_+(\mathbf{p}, \omega)$. Near $\omega/m = 0.1$, the rapid change of $\text{Re}\Sigma_+(\mathbf{p}, \omega)$ causes the quasi-dispersion relation to deviate from the free quark dispersion, as shown in Fig. 7.

3.2.3. Quark spectral function at intermediate temperature

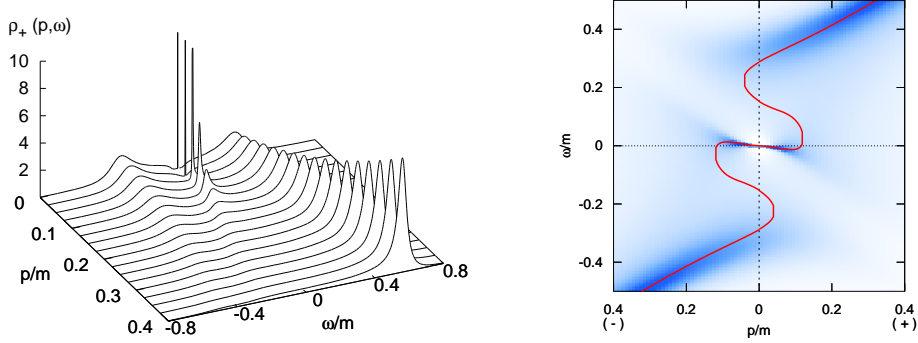
As T is raised further so that T becomes comparable with m , $\rho_\pm(\mathbf{p}, \omega)$ and $\omega_\pm(\mathbf{p})$ change drastically; note that the bosons become thermally excited with a considerable probability at such a temperature. In the left panels of Fig. 9, we plot $\rho_+(\mathbf{p}, \omega)$ for $T/m = 1.0, 1.4$ and 1.8 . We see that for $T/m = 1.0$, the quasi-particle peak starts to split near $|\mathbf{p}|/m = 0.15$. Also in this vicinity, there appear broad peaks both in the positive and negative energy regions for lower momenta. Thus the spectral function in the low-momentum region has *three peaks*.

A remark is in order here. Among the three peaks, that near the origin has no width, and thus it is difficult to read off the strength from Fig. 9. Here we note that the strength at

$$T/m = 1$$



$$T/m = 1.4$$



$$T/m = 1.8$$

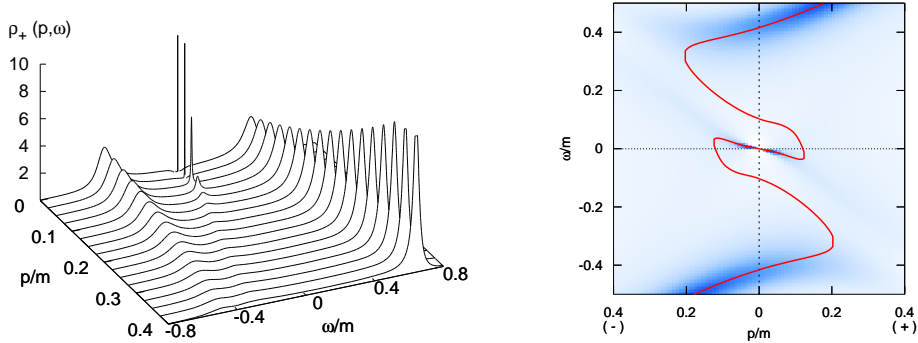


Fig. 9. The quark spectral function $\rho_+(\mathbf{p}, \omega)$ (left) and the quasi-dispersion relations $\omega_{\pm}(\mathbf{p})$ (right) for $T/m = 1.0, 1.4,$ and 1.8 from the top. In the right panels, the (ω, \mathbf{p}) dependence of $\rho_{\pm}(\mathbf{p}, \omega)$ is represented by the color density. ω_+ (ω_-) and ρ_+ (ρ_-) are shown in the right (left) halves of these panels. Note the direction of the momentum scale in the left half-plane is opposite to that of the right half-plane.

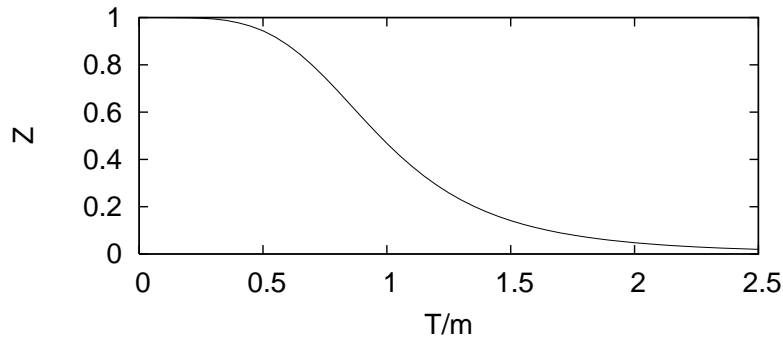


Fig. 10. The temperature dependence of the residue of the pole at the origin ($\omega = |\mathbf{p}| = 0$).

the origin is actually given by the residue of the Green functions, G_{\pm} : The residue is simply given by

$$Z(T) = [1 - \partial \text{Re} \Sigma_{\pm} / \partial \omega]^{-1}, \quad (3.17)$$

since the imaginary part, $\text{Im} \Sigma_{\pm}(\mathbf{p}, \omega)$, vanish at the origin. The T dependence of $Z(T)$ is shown in Fig. 10. It is seen that $Z(0) = 1$, as mentioned previously, and $Z(T)$ decreases gradually as T increases but is still considerably large for $T/m \sim 1$, and hence the three-peak structure of the spectral function is realized in this temperature region, as mentioned above.

In the high T limit, $Z(T)$ vanishes, and only two peaks remain in $\rho_{\pm}(\mathbf{p}, \omega)$. As we see below, these two peaks correspond to the normal quark quasi-particle and plasmino excitations obtained in the HTL approximation.

In the right panels of Fig. 9, we plot the quasi-dispersion relations and the (ω, p) dependence of the spectral function; the latter is represented by the (color) density. In these panels, ω_+ (ω_-) and ρ_+ (ρ_-) are shown in the right (left) halves of the figures. Note that the direction of the momentum scale in the left half plane is opposite to that in the right half plane. At $T/m = 1$, there is one quasi-dispersion curve for the entire momentum region. As T increases, the quasi-dispersion curve bends greatly forming ‘back-bending’ parts, and there eventually appear multi-valued quasi-dispersion relations for some momentum regions. At $T/m = 1.4$, the quasi-dispersion relation is five-valued at low momenta; note that this back-bending quasi-dispersion relation is acausal and unphysical. Only three of these values, however, are accompanied by peaks of the spectral function, as the quasi-dispersion relation $\omega_+(\mathbf{p})$ near the back-bending region does not form a peak in $\rho_+(\mathbf{p}, \omega)$ and is unphysical. The back-bending feature of the quasi-dispersion relation becomes more prominent as T increases further, as shown in the bottom-right panel in Fig. 9.

To understand the peculiar behavior of $\rho_+(\mathbf{p}, \omega)$ and $\omega_+(\mathbf{p})$ displayed in Fig. 9, we show $\Sigma_+(\mathbf{p}, \omega)$ at the intermediate temperature $T/m = 1.4$ in the right panel of Fig. 8. We see that the two peaks in $\text{Im} \Sigma_+(\mathbf{p}, \omega)$ become sharper than those for $T/m = 0.8$, shown in

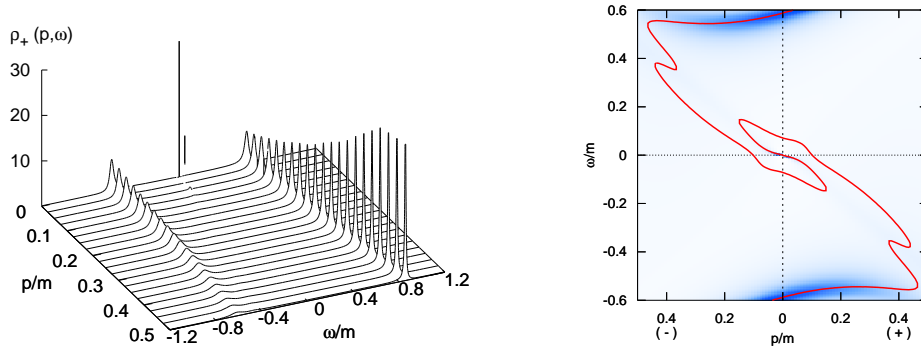


Fig. 11. The quark spectral function $\rho_+(\mathbf{p}, \omega)$ and the quasi-dispersion relation $\omega_{\pm}(\mathbf{p})$ for $T/m = 2.5$.

the left panel, and the oscillatory behavior of the real part for $\omega \sim 0$ also becomes more prominent. In order to determine the quasi-dispersion relation $\omega_+(\mathbf{p})$, i.e., the solutions of Eq. (2·10), from the figure, we plot the line $\omega - |\mathbf{p}|$, i.e. the l.h.s. of Eq. (2·10). In the top panel, we see that there appear five crossing points. The crossing points with the second and fourth largest ω , however, are located at the energies of the peak of $|\text{Im}\Sigma_+(\mathbf{p}, \omega)|$, and hence the spectral function does not form a peak there. For large momenta, the number of crossing points decreases, and eventually only one crossing point remains.

3.2.4. Quark spectral function at high temperature

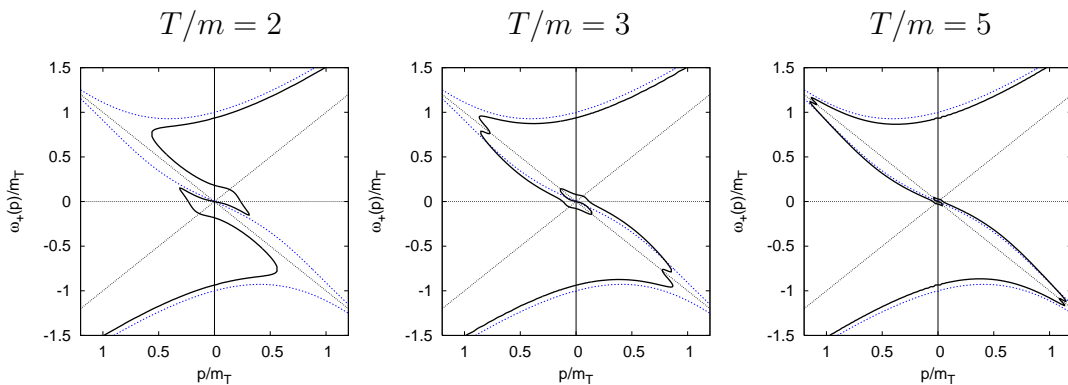


Fig. 12. The quasi-dispersion relations $\omega_{\pm}(\mathbf{p})$ for $T/m = 2, 3$ and 5 . All the values are in units of the thermal mass, $m_T = gT/4$. The dashed line represents the dispersion relation in the HTL approximation.

Here we examine the quark spectrum at higher temperatures. We plot $\rho_+(\mathbf{p}, \omega)$ and $\omega_{\pm}(\mathbf{p})$ for $T/m = 2.5$ in Fig. 11 as an example of the high-temperature case, i.e. $T \gg m$.

We see that two well-formed peaks appear in the positive and negative energy regions, while the peak near the origin immediately disappears as the momentum becomes finite. The curve representing the quasi-dispersion relation in the right panel is quite complicated. It should be noted that, however, the back-bending behavior of the quasi-dispersion relation is unphysical, and does not correspond to a peak of the spectral function, as mentioned previously. We plot the quasi-dispersion relation at several temperatures, $T/m = 2, 3$ and 5 , in the high- T region in Fig. 12, together with that in the HTL approximation with the thermal mass $m_T = gT/4$. From the figures, it is seen that our quasi-dispersion relation approaches that obtained in the HTL approximation as T increases; the two curves of $\omega_+(\mathbf{k})$ approach the quark quasi-particle and plasmino dispersion relations, respectively, with the thermal mass $m_T = gT/4$.*)

Here we note that there appears a continuous spectral bump near $\omega = 0$ in the space-like region in the HTL approximation, which is reminiscent of the spectral peak seen at intermediate temperatures in the space-like region near $\omega = 0$. We stress, however, that the physical origins of these peaks are completely different. The peak appearing at intermediate temperatures is due to the pole of the Green function, as shown in the previous subsection, while the bump in the HTL approximation is due to the Landau damping, and the quark propagator calculated in this approximation does not have a pole at $\omega = 0$.

3.3. Discussion of the three-peak structure of the spectral function for $T \sim m$

We have seen that the appearance of the three-peak structure for values of T comparable with the boson mass m is the most characteristic feature in the quark spectral function caused by the coupling with the massive boson. In this subsection, we attempt to elucidate the physical origin of the multi-peak structure. This discussion proceeds analogously to that⁷⁾ given for the origin of the three-peak structure caused by the soft mode of the chiral phase transition.

To understand the physical mechanism responsible for the three-peak structure of $\rho_+(\mathbf{p}, \omega)$, we first recall that there develop two peaks in $\text{Im}\Sigma_+$ at a positive and negative energy in this temperature region; the peak height here increases with T . As discussed in §3.1, these two peaks correspond to the decay processes depicted in (II) and (III) of Fig. 3, which are both Landau damping. The process (II) is the annihilation process of the incoming quark Q and the thermally excited antiquark into a boson in the thermal bath, $Q + \bar{q} \rightarrow b$, and its inverse process. Two remarks are in order here. First, the disappearance of an anti-quark implies the creation of a ‘hole’ in the thermally excited anti-quark distribution.¹⁴⁾ Second,

*) In fact, the spectrum in Fig. 12 does not exactly coincide with that in the HTL approximation because the coupling is not small. However, it is known that their difference is small at one-loop order.²³⁾

the creation of bosons in a thermal bath is enhanced in comparison with the case in vacuum by a statistical factor of $1 + n$, which becomes large when T is comparable to m . Thus, we see that the process (II) causes a virtual mixing between the quark and ‘anti-quark hole’ states through the coupling with the boson in a thermal bath, ^{*)} and as a result, the mixing is enhanced when $T/m \sim 1$.

The process (III) is another decay process of a quasi-quark state Q , which is now understood to be a mixed state of quarks and antiquark-holes, into an on-shell quark via a collision with a thermally excited boson: $Q + b \rightarrow q$ and its inverse process, $q \rightarrow Q + b$. As is seen from the left panel of Fig. 2, the energy involved in probable processes occurring at small momenta is negative for the process (III). These processes again give rise to a mixing of a quasi-quark and an anti-quark hole state. As seen from the Bose-Einstein distribution function n , thermally excited bosons are abundant when T approaches m .

A similar interpretation applies to the anti-quark sector, $\text{Im}\Sigma_-(\mathbf{p}, \omega)$, if the quark and anti-quark hole are replaced by an anti-quark and a quark hole, respectively. Thus, the process corresponding to (II) in Fig. 3 is $\bar{Q} + q \rightarrow b$, where q denotes a thermally excited quark, for instance. For this reason, from this point we only consider the quark sector.

The mechanism for the mixing of the quark and hole state can also be characterized as a *resonant scattering*,²⁰⁾ which was originally introduced to understand the non-Fermi liquid behavior of fermions just above the critical temperature of the superconducting transition.^{19),20)} In fact, we have seen that the process (II) in Fig. 3 includes a scattering process of the quark by a massive boson, thus creating a hole state in the thermally distributed anti-quark states: $Q \rightarrow \bar{q}_h + b$. Such a process is called resonant scattering.²⁰⁾ Note that the most probable process for finite T involves the lowest energy state of the boson, i.e., a rest boson with a energy m . The energy conservation law in the most probable case for the above process is $\omega_Q(\mathbf{p}) + \omega_{\bar{q}}(-\mathbf{p}) = m$, or equivalently,

$$\omega_Q(\mathbf{p}) = m - \omega_{\bar{q}}(-\mathbf{p}). \quad (3.18)$$

This equation actually represents the energy-momentum relation for the particles involved in the state mixing. Thus we see that the physical energy spectrum is obtained as a result of the level repulsion between the energies $\omega_q(\mathbf{p}) = |\mathbf{p}|$ and $m - \omega_{\bar{q}}(-\mathbf{p}) = m - |\mathbf{p}|$ in the perturbative picture. This situation is depicted in the upper-right part of the right panel in Fig. 13.

Similarly, the process (III) in Fig. 3 includes the process $q \rightarrow Q + b$, and the energy-

^{*)} We remark that quark number conservation is not violated with this mixing, because an ‘anti-quark hole’ has a positive quark number.

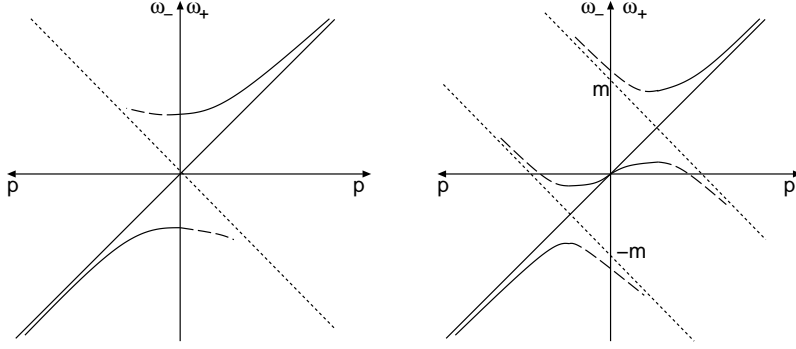


Fig. 13. Typical peak position of the spectral functions in the case of level mixing at the origin (left) and away from the origin (right). The long dashed curves show that the strength of the spectrum is becoming weaker. The solid line represents the free quark and antiquark dispersion relations, and the dotted line the antiquark hole and quark hole dispersion relations. Level repulsion takes place at the intersection point of these two lines.

momentum conservation law for this process for the most probable case is

$$-\omega_q(\mathbf{p}) = -m + \omega_Q(\mathbf{p}). \quad (3.19)$$

Thus, the physical energy spectrum is obtained as a result of the level repulsion between the energies $-|\mathbf{p}|$ and $-m + |\mathbf{p}|$. This situation is also depicted in the lower-right part of the right panel in Fig. 13.

We thus find that at temperatures satisfying $T/m \sim 1$, owing to the finite boson mass, the level repulsions occur far from the origin, and then the quasi-dispersion relations are bent twice, or two gap-like structures in the quark spectrum are formed at positive and negative energies, as shown in the right panel of Fig. 13.

It is interesting to consider the high temperature limit, $T \gg m$, or $m/T \sim 0$. In this case, the effect of the boson mass can be ignored, and the resonant scattering occurs only once at the origin ($\omega = |\mathbf{p}| = 0$), since the energy levels which are to be repelled cross only there. Then the situation becomes that represented in the left panel of Fig. 13.

It has been shown⁷⁾ that the quark spectral function possesses a three-peak structure near T_c of the chiral transition when the chiral soft mode⁴⁾ is incorporated into the quark self-energy. As was described in the Introduction, the soft modes behave like a massive elementary boson with a mass $m_\sigma^*(T)$ as T approaches T_c , i.e. $\omega_{\text{soft}} \sim \sqrt{\mathbf{p}^2 + m_\sigma^*(T)^2}$, and hence the quark spectra studied in Ref. 7) are essentially the same as that treated in this section. We also note that as T is lowered toward T_c , $m_\sigma^*(T)$ tends to vanish, and hence the ratio $T/m_\sigma^*(T)$ becomes large. Thus the quark spectrum approaches that in the $T/m \rightarrow \infty$ limit of the present work.⁷⁾

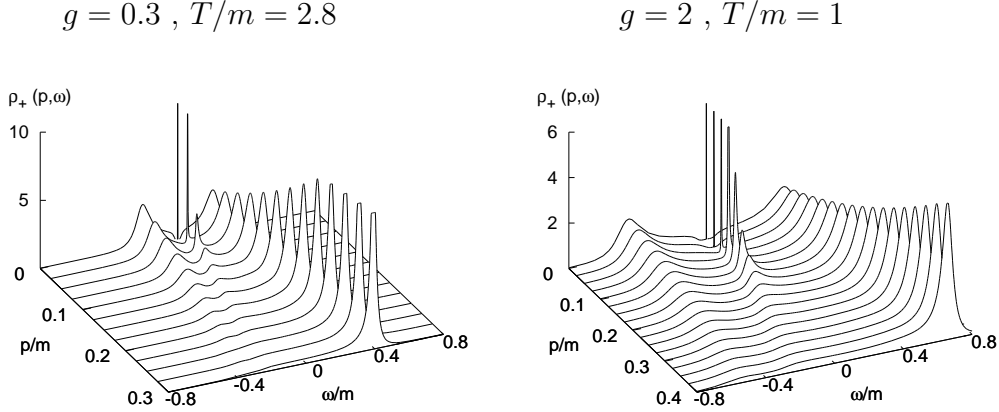


Fig. 14. The quark spectral functions $\rho_+(\mathbf{p}, \omega)$ for $g = 0.3, T/m = 2.8$ and $g = 2, T/m = 1$.

3.4. Quark spectral function for various coupling constants

We have derived the quark spectrum with the fixed coupling $g = 1$, and we have found novel three-peak structure at intermediate temperatures. How do these features change as g is varied? In the previous subsections, we pointed out that the Landau damping, which induces the two peaks in $\text{Im}\Sigma^R(\mathbf{p}, \omega)$, plays an essential role in creating the three-peak structure in the quark spectrum. Because $\Sigma^R(\mathbf{p}, \omega)/g^2$ is independent of g at one-loop order, we conjecture that the three-peak structure in the quark spectrum would not be affected qualitatively even if we varied the coupling g . We confirmed numerically that this is indeed the case: There appears similar three-peak structure in the quark spectrum for all values of g that we considered, although the temperature at which the clear three-peak structure appears depends on g .

In Fig. 14, we plot the quark spectral function $\rho_+(\mathbf{p}, \omega)$ with $g = 0.3$ and 2 , for values of T where a clear three-peak structure is seen. The spectral function possesses a single-peak structure at values of T lower than in the case considered in Fig. 14, and it approaches the two-peak structure at higher T . It is notable that for larger g , the three-peak structure appears at lower T and the distance between the peaks becomes larger.

§4. Quark spectrum in a Yukawa model with a massive vector (axial-vector) boson

In this section, we investigate the quark spectrum using a Yukawa model with a massive vector (axial-vector) boson and show that the three-peak structure of the quark spectral function is obtained.

We start from the following Lagrangian, composed of a massless quark ψ and vector

boson field V_μ :

$$\mathcal{L} = \bar{\psi}(i\cancel{\partial} - ig\gamma^\mu V_\mu)\psi + \mathcal{L}_v. \quad (4.1)$$

We consider the following simplest form for the Lagrangian of the massive vector field, \mathcal{L}_v :

$$\mathcal{L}_v = -\frac{1}{4}F_{\mu\nu}F^{\mu\nu} + \frac{1}{2}m^2V_\mu V^\mu, \quad (4.2)$$

with the field strength $F_{\mu\nu} = \partial_\mu V_\nu - \partial_\nu V_\mu$.

As in the case for the scalar boson, we find that the replacement of the vector boson with an axial-vector boson does not lead to any difference in the quark spectrum in the perturbation theory in this work.

4.1. Quark self-energy

At one-loop order, the quark self-energy in the imaginary time formalism is given by

$$\tilde{\Sigma}(\mathbf{p}, i\omega_m) = -g^2 T \sum_n \int \frac{d^3\mathbf{k}}{(2\pi)^3} \gamma^\mu \mathcal{G}_0(\mathbf{k}, i\omega_n) \gamma^\nu \mathcal{D}_{\mu\nu}(\mathbf{p} - \mathbf{k}, i\omega_m - i\omega_n), \quad (4.3)$$

with the Matsubara propagator for the massive vector boson,

$$\mathcal{D}_{\mu\nu}(i\nu_n, \mathbf{p}) = -\frac{g_{\mu\nu} - \tilde{p}_\mu \tilde{p}_\nu / m^2}{\tilde{p}_\mu \tilde{p}^\mu - m^2}, \quad (4.4)$$

where $\tilde{p}_\mu = (i\nu_n, \mathbf{p})$. The propagator for this vector boson, which is obtained from Eq. (4.2), is called the Proca propagator.²⁴⁾ It is known that the massless limit of Eq. (4.4) cannot be taken, because of the lack of gauge invariance of Eq. (4.2). As we see below, this property causes a problem in the the high temperature limit, $T/m \rightarrow \infty$, because this limit also represents the massless limit with fixed T . One should describe a boson field in the Stuckelberg formalism,²⁴⁾ which has a massless limit, if we study the spectrum at high T . In this work, because we explore the qualitative effect of the phenomenological massive vector boson on the quark spectrum at intermediate T , we do not consider this problem associated with the Proca propagator.

For coupling with an axial-vector boson, the self-energy has the same form as Eq. (4.3), because the γ_5 matrices in the vertices cancel out in the case of a massless quark propagator \mathcal{G}_0 . Therefore, the following results hold also for the coupling with an axial-vector boson, as mentioned above.

Carrying out the summation over the Matsubara modes in Eq. (4.3) and applying the analytic continuation $i\omega_n \rightarrow \omega + i\eta$ (see Appendix B for details), we obtain

$$\Sigma^R(\mathbf{p}, \omega) = g^2 \sum_{s,t=\pm} t \int \frac{d^3\mathbf{k}}{(2\pi)^3} \frac{\gamma^\mu \Lambda_s(\mathbf{k}) \gamma^0 \gamma^\nu}{2E_b} \left(g_{\mu\nu} - \frac{q_\mu q_\nu}{m^2} \right) \frac{f(sE_f) + n(-tE_b)}{\omega + i\eta - sE_f - tE_b}, \quad (4.5)$$

with $q_\mu = (\omega - E_f, \mathbf{p} - \mathbf{k})$. In order to eliminate the ultraviolet divergence in Eq. (4.5), we employ the same strategy as in the previous section: We first divide Eq. (4.5) into T -independent and T -dependent parts as $\Sigma^R(\mathbf{p}, \omega) = \Sigma^R(\mathbf{p}, \omega)_{T=0} + \Sigma^R(\mathbf{p}, \omega)_{T \neq 0}$ and calculate $\Sigma^R(\mathbf{p}, \omega)_{T=0}$ while imposing the renormalization condition.

In the present case, however, unlike in the previous section, the T -independent part, $\Sigma^R(\mathbf{p}, \omega)_{T=0}$, includes a divergence in the term proportional to \not{p}^3 , and the on-shell renormalization condition alone cannot eliminate the divergence (see Appendix C). This is due to the bad ultraviolet behavior coming from the Proca propagator $D_{\mu\nu}^R$. Here we impose the renormalization condition $\partial^3 \Sigma^R(p)/\partial \not{p}^3|_{\not{p}=0} = 0$ to eliminate this divergence and obtain the following renormalized form:

$$\begin{aligned} \Sigma^R(p)_{T=0} = & \frac{g^2}{32\pi^2} \not{p} \left(\frac{P^2 + 2m^2}{m^2} \frac{(P^2 - m^2)^2}{P^4} \log \left| \frac{m^2 - P^2}{m^2} \right| - \frac{5}{6} \frac{P^2}{m^2} - 2 + 2 \frac{m^2}{P^2} \right) \\ & - i \frac{g^2}{32\pi^2} \not{p} \frac{P^2 + 2m^2}{m^2} \frac{(P^2 - m^2)^2}{P^4} \epsilon(p_0) \theta(P^2 - m^2). \end{aligned} \quad (4.6)$$

The T -dependent part $\Sigma^R(\mathbf{p}, \omega)_{T \neq 0}$ can be calculated using the same procedure as in the previous section; i.e., we first calculate the imaginary part $\text{Im} \Sigma^R(\mathbf{p}, \omega)_{T \neq 0}$ and then derive the real part using the dispersion relation, Eq. (3.5).

From Eq. (4.5), we obtain

$$\begin{aligned} \text{Im} \Sigma^R(\mathbf{p}, \omega) = & -\pi g^2 \int \frac{d^3 \mathbf{k}}{(2\pi)^3} \frac{\gamma^\mu \Lambda_s(\mathbf{k}) \gamma^0 \gamma^\nu}{2E_b} \left(g_{\mu\nu} - \frac{q_\mu q_\nu}{m^2} \right) \\ & \times \{ -(1+n-f)\delta(\omega - E_f - E_b) - (n+f)\delta(\omega + E_f - E_b) \\ & + (n+f)\delta(\omega - E_f + E_b) + (1+n-f)\delta(\omega + E_f + E_b) \}, \end{aligned} \quad (4.7)$$

with $n = n(E_b)$ and $f = f(E_f)$. The four terms in Eq. (4.7) have the same statistical factors and delta functions as those in Eq. (3.6), which means that the decay processes of the quasi-particles described by these terms can be understood diagrammatically from Fig. 3. The region in the energy-momentum plane where each term has a finite value is the same as in the case of Fig. 2.

For $\mathbf{p} = \mathbf{0}$, we obtain

$$\text{Im} \Sigma_\pm(\mathbf{p} = \mathbf{0}, \omega) = -\frac{g^2}{32\pi} \frac{\omega^2 + 2m^2}{m^2} \frac{(\omega^2 - m^2)^2}{\omega^3} \left(\coth \frac{\omega^2 + m^2}{4T\omega} + \tanh \frac{\omega^2 - m^2}{4T\omega} \right). \quad (4.8)$$

Equation (4.8) differs from Eq. (3.11) in the Yukawa model with a scalar boson by a factor of $(\omega^2 + 2m^2)/m^2$. For small energy, i.e. $\omega \lesssim m$, this term approximately gives an overall

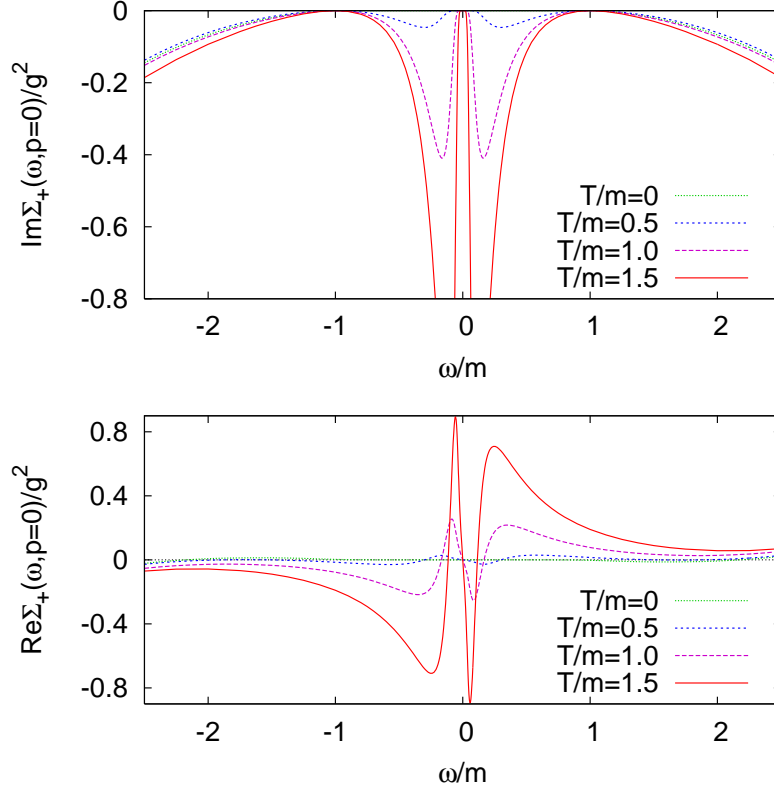


Fig. 15. The imaginary and real parts of the self-energy, $\Sigma_+(\mathbf{p}, \omega)$, at zero momentum for several temperatures.

factor of 2. Therefore, we expect that the two-peak structure of $\text{Im}\Sigma_{\pm}(\mathbf{p} = 0, \omega)$ caused by the Landau damping at $|\omega| < m$ and, hence, the three-peak structure in the quark spectral function is not qualitatively altered even in the present case. For large ω , however, the factor behaves as ω^2/m^2 , which makes Eq. (4.8) much larger than Eq. (3.11) for $|\omega| \gg m$. This leads to a difference between the scalar and the vector bosons at very high T .

4.2. Quark spectrum at intermediate temperatures

In Fig. 15, we plot the imaginary and real parts of $\Sigma_+(\mathbf{p}, \omega)$ for $\mathbf{p} = 0$ at $T/m = 0, 0.5, 1$ and 1.5 . We fix the coupling constant at $g = 1$. As can be deduced from the above discussion, the qualitative features of both parts for $|\omega|/m < 1$ are quite similar to those in Fig. 4: There are two clear peaks in $\text{Im}\Sigma_+$ for $|\omega|/m < 1$ and oscillating behavior in $\text{Re}\Sigma_+(\mathbf{p} = 0, \omega)$, and they grow rapidly as T increases. For $|\omega|/m > 1$, it is seen that $|\text{Im}\Sigma_+(\mathbf{p} = 0, \omega)|$ grows more rapidly than in the Yukawa model with the scalar boson shown in Fig. 4.

In Fig. 16, we plot $|\text{Im}\Sigma_+(\mathbf{p}, \omega)|$ in the energy-momentum plane for $T/m = 1.5$. We see that the qualitative features of $|\text{Im}\Sigma_+(\mathbf{p}, \omega)|$ are again almost the same as those in Fig. 5 for $|\omega|/m \lesssim 1$.

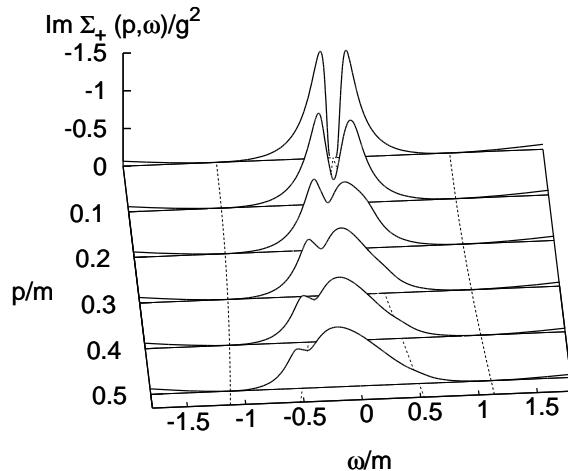


Fig. 16. The imaginary part of the self-energy, $|\text{Im}\Sigma_+(\mathbf{p}, \omega)|$, for $T/m = 1.5$.

In Fig. 17, we plot the quark spectral function for $T/m = 0.4, 0.8, 1.0$ and 1.2 . It is seen that there appears a three-peak structure at intermediate temperatures, as found in the previous section. This is quite natural, and it would be expected from the behavior of the self-energy. A clear three-peak structure is formed at lower values of T than in the scalar boson case. This is because the term $(\omega^2 + 2m^2)/m^2$ in Eq. (4·8), which gives approximately a factor of 2 for $\omega \lesssim m$, tends to enhance the coupling constant g . As discussed in §3.4, the temperature at which the clear three-peak structure appears decreases for larger g .

4.3. Quark spectrum at high temperatures

Next, we plot the quark spectral function at higher temperatures, $T/m = 5$ and 10 , in Fig. 18. We find that the energy at the quasi-particle peak converges to a value near $\omega/m = 2.5$ as T/m increases for $\mathbf{p} = 0$. It is also noteworthy that the two peaks with finite thermal mass become obscure as T increases.

In order to understand this behavior of $\rho_+(\mathbf{p}, \omega)$ at higher T , in Fig. 19 we plot the self-energy for $T/m = 0, 5, 10$, and 15 . In the right figure, we plot the line $\text{Re}\Sigma_+ = \omega$ in order to see the quasi-dispersion relation. At $T = 0$, there exist three quasi-dispersion relations at $\omega = 0$ and near $\omega = \pm 10m$. The latter two solutions are unphysical.*⁾ In Fig. 19, it is also noteworthy that $\text{Re}\Sigma_+$ changes sign near $\omega = 2.5m$ for higher T . In fact, we can analytically prove that the zero of $\text{Re}\Sigma_+$ approaches $\omega = \sqrt{6}m$ in the high T limit (see Appendix D). Due to this property, the solution of the quasi-dispersion relation corresponding to the two peaks in Fig. 17 approaches $|\omega| = \sqrt{6}m$ at $\mathbf{p} = 0$ in the high T limit.

*⁾ These quasi-dispersion relations do not form a peak in the quark spectral function, because $|\text{Im}\Sigma^R|$ takes a large value there. We have confirmed that they also exist for very large values of ω in the model with a scalar boson in §3.

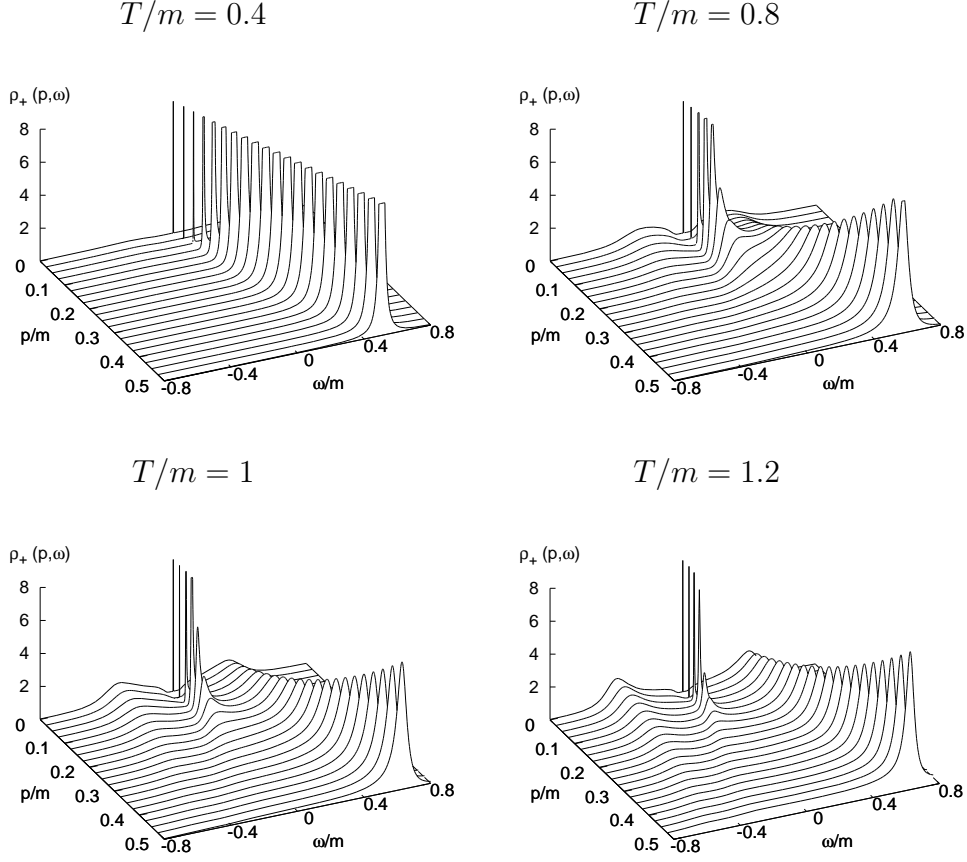


Fig. 17. The quark spectral function $\rho_+(\mathbf{p}, \omega)$ for $T/m = 0.4, 0.8, 1$ and 1.2 .

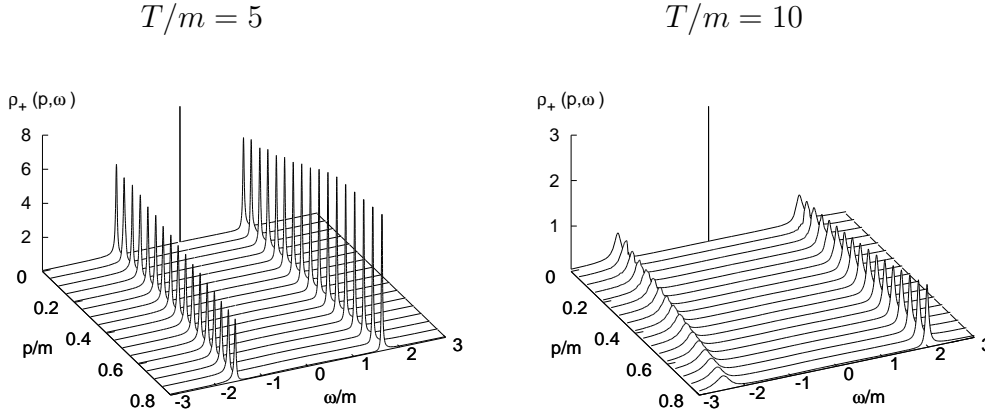


Fig. 18. The quark spectral function $\rho_+(\mathbf{p}, \omega)$ for $T/m = 5$ and 10 .

§5. Summary and concluding remarks

We have investigated the quasi-particle picture of a fermion, which we call a “quark” in this paper, employing Yukawa models composed of a massless quark and a massive boson

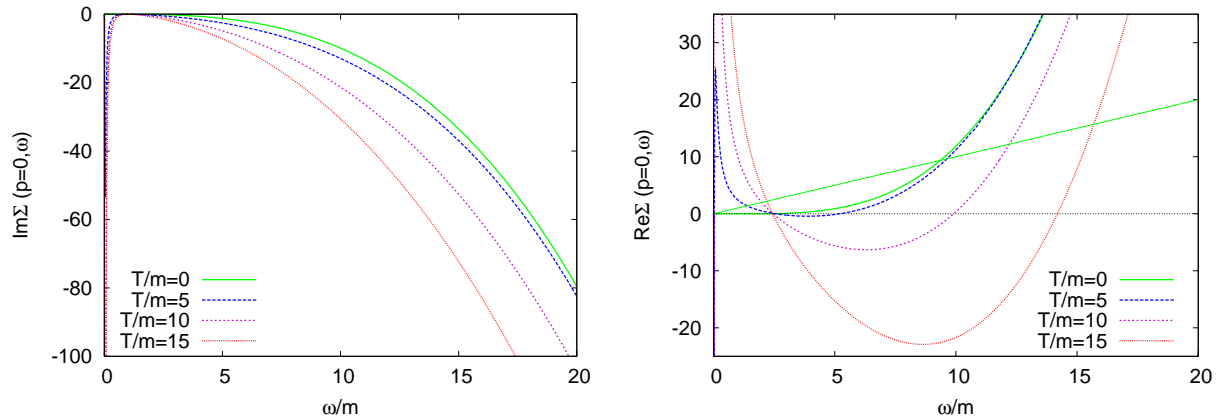


Fig. 19. The imaginary and real parts of the self-energy, $\Sigma_+(\mathbf{p}, \omega)$, at zero momentum for $T/m = 5, 10$ and 15 .

at finite temperature (T). We have considered four types of massive bosons, i.e., scalar, pseudoscalar, vector and axial-vector bosons, with a mass m , though there is no difference in the quark spectra for the scalar (vector) and pseudoscalar (axial-vector) bosons, because the quark is massless. The Proca formalism was employed for the vector boson. For both models, the quark self-energy was computed up to one-loop order, and the spectral function and quasi-dispersion relation of the quark were studied. We have found that the quark spectral function at low frequency and low momentum is significantly different from the free quark spectrum, and it has a three-peak structure at intermediate values of T , i.e., for $T/m \sim 1$. We have also found that the number of branches of the quasi-dispersion relation does not necessarily coincide with that of the peaks in the fermion spectral function when the imaginary part of the quark self-energy is large. We have shown that the two of the three peaks have finite thermal masses and approach the normal quasi-quark and plasmino excitations in the HTL approximation in the high T limit, while the strength of the peak at the origin becomes weaker and disappears in this limit. In the Yukawa model with a vector boson, we have found that the behavior of the spectral function is the same as that in the Yukawa model with a scalar boson up to $T \approx m$. In the high T limit, the spectrum in the Proca formalism does not approach that in the HTL approximation.

We have discussed the fact that the three-peak structure originates from the Landau damping, that is, the scattering processes of a quark and an antiquark hole of a thermally excited antiquark, and of an antiquark and a quark hole of a thermally excited quark. They cause the formation of energy gaps in the quark spectrum, owing to the level mixing between the quark (antiquark) and the hole of the thermally excited antiquarks (quarks). This leads to a level repulsion or gap in the resultant physical spectrum. These mixings can

be understood in terms of the resonant scattering^{19),20)} of the quasi-quarks off the bosons. In particular, owing to the mass of the boson, the level repulsion due to the resonant scattering occurs *twice* at different points in the energy-momentum plane, leading to the three-peak structure of the spectral function. This contrasts with the case of the quark spectrum coupled to a massless boson, such as a gauge boson, in which the resonant scattering occurs only at the origin in the energy-momentum plane and then leads to only two peaks, as in the spectrum in the HTL approximation.

Since there may exist bosonic excitations (even apart from gluons) coupled to quarks in the QGP phase,^{4),25),26)} it is plausible that the quark spectrum would have a three-peak structure in the QGP phase if the boson has a “mass” of the order of T ; if there exist several bosonic excitations with “masses” close to T , the quark spectral function may become a superposition of three-peak structures with various heights. Although the quark spectral function in QCD is a gauge-dependent quantity, the complex pole of the quark Green function is gauge invariant. For this reason, we conjecture that the peak structure of the quark spectral function reflects the complex pole of the Green function and will be seen in gauge theories, for example, QCD.

One interesting example of bosonic excitations which may affect the quasi-particle picture of the quarks in the QGP phase is the soft modes associated with the chiral transition.⁴⁾ The chiral soft mode is unique, because its effective mass $m_\sigma^*(T)$ may become as small as a few hundred MeV, and thus it can eventually be of the same order as T near T_c of the chiral transition if the phase transition is second order or weakly first order. In fact, it has been shown⁷⁾ that the chiral soft modes give rise to a three-peak structure in the quark spectrum just above T_c : In Ref. 7), the Nambu-Jona-Lasinio model is employed as a chiral model, and the quark spectral function is calculated incorporating the effect of the dynamically generated soft modes into the quark propagator. It is noteworthy that although the soft mode obtained in the dynamical model employed in Ref. 7) is a composite particle with a finite width and thus not an elementary boson, a clear three-peak structure is realized in the quark spectral function.

It would be interesting to investigate the effect in the change of the quark spectrum on various observables in the QGP phase. In particular, it would be intriguing to explore the dilepton production rate; because the quasiparticle peaks in the three-peak structure have low sound velocities, there can appear a sharp peak in the dilepton production rate owing to a mechanism similar to that causing the van Hove singularities.²⁷⁾ It would also be an interesting to consider the properties of mesonic excitations in the QGP phase composed of quarks having the spectrum obtained in this work.

We remark that a lattice QCD simulation of the quark spectrum would be, of course,

preferable, although this would require the performance of several tasks, such as the gauge fixing, carrying out the chiral extrapolation and using dynamical (chiral) fermions to elucidate the effects of the chiral soft modes.

Contributions of higher order terms such as more than one-loop diagrams, which are not taken into account in the present, may affect the peak structure of the spectrum. In condensed matter physics, some corrections based on self-consistency conditions are proposed²⁸⁾ and their possible effects on the quark spectrum near the color superconducting phase transition are commented in Ref. 17).

Because the present investigation is based on simple but generic Yukawa models with a massive scalar and vector boson, the results obtained here should apply to various systems at finite T composed of a light fermion and a massive boson, in addition to QCD matter in the QGP phase. One such system is the excitation spectra of neutrinos coupled to weak bosons at high T near the masses of the weak bosons.²⁹⁾ The investigation of a such system would be carried out exclusively in terms of the neutrino quasi-dispersion relations.

In this paper, we have considered only massless quarks. A finite quark mass should affect the formation of the three-peak structure in the quark spectral function. Thus, the incorporation of the quark mass effect is important for describing the chiral transition precisely, because the order of the transition, and hence, the quark spectrum near the critical point are sensitive to the quark mass. A finite quark mass also leads to a difference between the scalar (vector) and pseudoscalar (axial-vector) boson cases, and may suppress the three-peak structure, because it does not appear in Ref. 21), where a massive quark spectrum coupled with a massless boson is studied at finite T . Detailed study of such a effect is now under way and will be reported elsewhere.³⁰⁾ The finite chemical potential may also alter the three-peak structure because antiquarks in medium are fewer in this case, and thus, mixing between the quark and the antiquark-hole will be suppressed. Such a study is also now under investigation.³¹⁾

Acknowledgements

M. K. is grateful to Y. Hidaka and R. D. Pisarski for useful discussions. He also acknowledges L. McLerran and F. Karsch for their interest in this work. T. K. acknowledges B. Müller for valuable comments. Y. N. thanks M. Harada for useful comments. M. K. is supported by a Special Postdoctoral Research Program of RIKEN. T. K. is supported by a Grant-in-Aid for Scientific Research by Monbu-Kagakusyo of Japan (No. 17540250). Y. N. is supported by the 21st Century COE Program at Nagoya University and a Grand-in-Aid for Scientific Research by Monbu-Kagakusyo of Japan (No. 18740140). This work is supported

by the Grant-in-Aid for the 21st Century COE ‘‘Center for Diversity and Universality in Physics’’ of Kyoto University.

Appendix A

— Quark Self-Energy in the Yukawa Model with Scalar Coupling —

In this appendix, we summarize the calculation of the quark self-energy in the model with the scalar boson given in Eq. (3.2),

$$\tilde{\Sigma}(\mathbf{p}, i\omega_m) = -g^2 T \sum_n \int \frac{d^3 \mathbf{k}}{(2\pi)^3} \mathcal{G}_0(\mathbf{k}, i\omega_n) \mathcal{D}(\mathbf{p} - \mathbf{k}, i\omega_m - i\omega_n), \quad (\text{A}\cdot 1)$$

where

$$\mathcal{G}_0(\mathbf{k}, i\omega_n) = \frac{1}{i\omega_n \gamma^0 - \mathbf{k} \cdot \boldsymbol{\gamma}} = \sum_s \Lambda_s(\mathbf{k}) \gamma^0 \frac{1}{i\omega_n - sE_f}, \quad (\text{A}\cdot 2)$$

$$\mathcal{D}(\mathbf{k}, i\nu_n) = \frac{1}{(i\nu_n)^2 - \mathbf{k}^2 - m^2} = \sum_t t \frac{1}{2E_b(i\nu_n - tE_b)} \quad (\text{A}\cdot 3)$$

are the free propagators of the quark and the scalar boson, respectively. Here, $\Lambda_{\pm}(\mathbf{k}) = (1 \pm \gamma^0 \boldsymbol{\gamma} \cdot \hat{\mathbf{k}})/2$ are the projection operators onto positive and negative energies, respectively. Substituting Eqs. (A.2) and (A.3) into Eq. (A.1), we have

$$\tilde{\Sigma}(\mathbf{p}, i\omega_m) = -g^2 \sum_{s,t=\pm} T \sum_n \int \frac{d^3 \mathbf{k}}{(2\pi)^3} \frac{t \Lambda_s(\mathbf{k}) \gamma^0}{2E_b} \frac{1}{i\omega_n - sE_f} \frac{1}{i\omega_m - i\omega_n - tE_b}, \quad (\text{A}\cdot 4)$$

with $E_f = |\mathbf{k}|$ and $E_b = \sqrt{(\mathbf{p} - \mathbf{k})^2 + m^2}$. Carrying out the summation over the Matsubara modes n and applying the analytic continuation $i\omega_m \rightarrow \omega + i\eta$ in Eq. (A.4), we obtain the retarded self-energy and its imaginary part:

$$\Sigma^R(\mathbf{p}, \omega) = -g^2 \sum_{s,t=\pm} \int \frac{d^3 \mathbf{k}}{(2\pi)^3} \frac{t \Lambda_s(\mathbf{k}) \gamma^0}{2E_b} \frac{f(sE_f) + n(-tE_b)}{\omega - sE_f - tE_b + i\eta}, \quad (\text{A}\cdot 5)$$

$$\text{Im} \Sigma^R(\mathbf{p}, \omega) = \pi g^2 \sum_{s,t=\pm} \int \frac{d^3 \mathbf{k}}{(2\pi)^3} \frac{t \Lambda_s(\mathbf{k}) \gamma^0}{2E_b} \{f(sE_f) + n(-tE_b)\} \delta(\omega - sE_f - tE_b). \quad (\text{A}\cdot 6)$$

Equations (3.3) and (3.6) are obtained by carrying out the summations over s and t in Eqs. (A.5) and (A.6), respectively.

We next decompose the self-energy with the projection operators into $\Sigma^R(\mathbf{p}, \omega) = \Sigma_+(\mathbf{p}, \omega) \Lambda_+(\mathbf{p}) \gamma^0 + \Sigma_-(\mathbf{p}, \omega) \Lambda_-(\mathbf{p}) \gamma^0$. The imaginary part of $\Sigma_+(\mathbf{p}, \omega)$ is calculated in the following way:

$$\text{Im} \Sigma_+(\mathbf{p}, \omega) = \frac{1}{2} \text{Tr} [\text{Im} \Sigma^R(\mathbf{p}, \omega) \Lambda_+(\mathbf{p}) \gamma^0]$$

$$= \pi g^2 \sum_{s,t=\pm} \int \frac{d^3 \mathbf{k}}{(2\pi)^3} \frac{1 - s\hat{\mathbf{p}} \cdot \hat{\mathbf{k}}}{4tE_b} \{f(sE_f) + n(-tE_b)\} \delta(\omega - sE_f - tE_b) \quad (\text{A}\cdot 7)$$

$$= -\frac{g^2}{32\pi \mathbf{p}^2} \sum_{s,t=\pm} st \int dE_f \int_{e_-}^{e_+} dE_b [(|\mathbf{p}| - sE_f)^2 - E_b^2 + m^2] \\ \times \{f(sE_f) + n(-tE_b)\} \delta(\omega - sE_f - tE_b) \\ = -\frac{g^2}{32\pi \mathbf{p}^2} \sum_{s,t=\pm} st \int dE_f [(|\mathbf{p}| + \omega - 2E_f)(|\mathbf{p}| - \omega) + m^2] \\ \times \{f(sE_f) + n(sE_f - \omega)\} \int_{e_-}^{e_+} dE_b \delta(\omega - sE_f - tE_b), \quad (\text{A}\cdot 8)$$

where in the third equality we have used the relations

$$\hat{\mathbf{p}} \cdot \hat{\mathbf{k}} = \frac{\mathbf{p}^2 + E_f^2 - E_b^2 + m^2}{2|\mathbf{p}|E_f}, \quad (\text{A}\cdot 9)$$

$$\int \frac{d^3 \mathbf{k}}{(2\pi)^3} = \frac{1}{4\pi^2 |\mathbf{p}|} \int dE_f E_f \int_{e_-}^{e_+} dE_b E_b, \quad (\text{A}\cdot 10)$$

with $e_{\pm} = \sqrt{(|\mathbf{p}| \pm E_f)^2 + m^2}$.

In the time-like region, one of the four terms in Eq. (A·8) takes a finite value (see Fig. 2). After some algebra, it is found that all these terms in the time-like region are reduced to the following simple form:

$$\text{Im}\Sigma_+(\mathbf{p}, \omega) = -\frac{g^2}{32\pi \mathbf{p}^2} \int_{E_f^+}^{E_f^-} dE_f [(|\mathbf{p}| + \omega - 2E_f)(|\mathbf{p}| - \omega) + m^2] \\ \times \{f(sE_f) + n(sE_f - \omega)\}, \quad (\text{A}\cdot 11)$$

with

$$E_f^{\pm} = \frac{\omega^2 - \mathbf{p}^2 - m^2}{2(\omega \pm |\mathbf{p}|)}. \quad (\text{A}\cdot 12)$$

In the space-like region, the two terms corresponding to (II) and (III) in Fig. 3 take finite values, and Eq. (A·8) yields

$$\text{Im}\Sigma_+(\mathbf{p}, \omega) \\ = -\frac{g^2}{32\pi \mathbf{p}^2} \left[\int_{E_f^+}^{-\infty} dE_f - \int_{\infty}^{E_f^-} dE_f \right] [(|\mathbf{p}| + \omega - 2E_f)(|\mathbf{p}| - \omega) + m^2] \\ \times \{f(E_f) + n(E_f - \omega)\} \\ = -\frac{g^2}{32\pi \mathbf{p}^2} \left[\int_{E_f^+}^{E_f^-} dE_f - \int_{-\infty}^{\infty} dE_f \right] [(|\mathbf{p}| + \omega - 2E_f)(|\mathbf{p}| - \omega) + m^2]$$

$$\begin{aligned}
& \times \{f(E_f) + n(E_f - \omega)\} \\
= & -\frac{g^2}{32\pi\mathbf{p}^2} \int_{E_f^+}^{E_f^-} dE_f [(|\mathbf{p}| + \omega - 2E_f)(|\mathbf{p}| - \omega) + m^2] \{f(E_f) + n(E_f - \omega)\} \\
& - \frac{\pi g^2 T^2}{32} \frac{|\mathbf{p}| - \omega}{\mathbf{p}^2} - \frac{g^2}{32\pi} \frac{\omega[|\mathbf{p}|(|\mathbf{p}| - \omega) + m^2]}{\mathbf{p}^2}, \tag{A.13}
\end{aligned}$$

where we have used the integral formulae

$$\int_{-\infty}^{\infty} d\epsilon [f(\epsilon) + n(\epsilon - \omega)] = -\omega, \tag{A.14}$$

$$\int_{-\infty}^{\infty} d\epsilon \epsilon [f(\epsilon) - n(\epsilon - \omega)] = \frac{\pi^2 T^2}{2} + \frac{\omega^2}{2}. \tag{A.15}$$

Equations (A.11) and (A.13) are combined to give

$$\begin{aligned}
& \text{Im}\Sigma_+(\mathbf{p}, \omega) \\
= & -\frac{g^2}{32\pi\mathbf{p}^2} \int_{E_f^+}^{E_f^-} dE_f [(|\mathbf{p}| + \omega - 2E_f)(|\mathbf{p}| - \omega) + m^2] \{f(E_f) + n(E_f - \omega)\} \\
& - \left\{ \frac{\pi g^2 T^2}{32} \frac{|\mathbf{p}| - \omega}{\mathbf{p}^2} + \frac{g^2}{32\pi} \frac{\omega[|\mathbf{p}|(|\mathbf{p}| - \omega) + m^2]}{\mathbf{p}^2} \right\} \theta(\mathbf{p}^2 - \omega^2). \tag{A.16}
\end{aligned}$$

For $\mathbf{p} = \mathbf{0}$, from Eq. (A.7) we obtain

$$\text{Im}\Sigma_{\pm}(\mathbf{0}, \omega) = -\frac{g^2}{64\pi} \frac{(\omega^2 - m^2)^2}{\omega^3} \left(\coth \frac{\omega^2 + m^2}{4T\omega} + \tanh \frac{\omega^2 - m^2}{4T\omega} \right). \tag{A.17}$$

The T -independent part of $\text{Im}\Sigma_+(\mathbf{p}, \omega)$ is given by the $T = 0$ limit of Eq. (A.16). In this case, the integral in Eq. (A.16) can be performed analytically, and we obtain

$$\text{Im}\Sigma_+(\mathbf{p}, \omega)_{T=0} = -\frac{g^2}{32\pi} (\omega - |\mathbf{p}|) \frac{(P^2 - m^2)^2}{P^4} \text{sgn}(\omega) \theta(P^2 - m^2), \tag{A.18}$$

with $P^2 = \omega^2 - \mathbf{p}^2$.

The T -dependent part, $\text{Im}\Sigma_+^R(\mathbf{p}, \omega)_{T \neq 0}$, is obtained through the replacement of the distribution function in the curly brackets in Eq. (A.8) as

$$f(E_f) + n(\omega - E_f) \rightarrow n(\omega - E_f) + f(E_f) + \epsilon(\omega) \theta(P^2 - m^2). \tag{A.19}$$

Appendix B

— Quark Self-Energy in the Yukawa Model with Vector Coupling —

The self-energy of the quark in a Yukawa model with a massive vector boson is given by Eq. (4.3) as

$$\tilde{\Sigma}(\mathbf{p}, i\omega_m) = -g^2 T \sum_n \int \frac{d^3\mathbf{k}}{(2\pi)^3} \gamma^\mu \mathcal{G}_0(\mathbf{k}, i\omega_n) \gamma^\nu \mathcal{D}_{\mu\nu}(\mathbf{p} - \mathbf{k}, i\omega_m - i\omega_n), \tag{B.1}$$

with the Proca propagator $\mathcal{D}_{\mu\nu}$ defined in Eq. (4.4). Carrying out the summation over the Matsubara modes n and applying the analytic continuation $i\omega_m \rightarrow \omega + i\eta$, the retarded self-energy $\Sigma^R(\mathbf{p}, \omega)$ is obtained as Eq. (4.5), and the imaginary part is given by

$$\begin{aligned} \text{Im}\Sigma^R(\mathbf{p}, \omega) &= -\pi g^2 \sum_{s,t=\pm} t \int \frac{d^3\mathbf{k}}{(2\pi)^3} \frac{\gamma^\mu \Lambda_s(\mathbf{k}) \gamma^0 \gamma^\nu}{2E_b} \left(g_{\mu\nu} - \frac{q_\mu q_\nu}{m^2} \right) \\ &\quad \times \{f(sE_f) + n(-tE_b)\} \delta(\omega - sE_f - tE_b), \end{aligned} \quad (\text{B}\cdot 2)$$

with $E_f = |\mathbf{k}|$, $E_b = \sqrt{(\mathbf{p} - \mathbf{k})^2 + m^2}$ and $q_\mu = (tE_b, \mathbf{p} - \mathbf{k})$. The quark sector of Eq. (B.2) gives

$$\begin{aligned} \text{Im}\Sigma_+(\mathbf{p}, \omega) &= \text{Tr} [\text{Im}\Sigma^R(\mathbf{p}, \omega) \Lambda_+(\mathbf{p}) \gamma^0] \\ &= \pi g^2 \sum_{s,t=\pm} t \int \frac{d^3\mathbf{k}}{(2\pi)^3} \frac{t}{2E_b} \left[\frac{(tE_b - \hat{s}\hat{\mathbf{k}} \cdot \mathbf{q})(tE_b - \hat{\mathbf{p}} \cdot \mathbf{q})}{m^2} - \frac{1 - \hat{s}\hat{\mathbf{k}} \cdot \hat{\mathbf{p}}}{2} \right] \\ &\quad \times \{f(sE_f) + n(-tE_b)\} \delta(\omega - sE_f - tE_b) \\ &= \frac{g^2}{32\pi \mathbf{p}^2 m^2} \sum_{s,t=\pm} st \int dE_f [(\mathbf{p}^2 - \omega^2 + m^2) ((|\mathbf{p}| - \omega)^2 - 2m^2) \\ &\quad + 2sE_f(\mathbf{p}^2 - \omega^2 + 2m^2)(|\mathbf{p}| - \omega)] \int_{e^-}^{e^+} dE_b \delta(\omega - sE_f - tE_b) \\ &= -\frac{g^2}{32\pi \mathbf{p}^2 m^2} \int_{E_f^+}^{E_f^-} d\epsilon [-(P^2 - m^2) \{(|\mathbf{p}| - \omega)^2 - 2m^2\} \\ &\quad + 2\epsilon(\omega - |\mathbf{p}|)(P^2 - 2m^2)] \{f(\epsilon) + n(\epsilon - \omega)\} \\ &\quad - \frac{g^2}{32\pi \mathbf{p}^2 m^2} \theta(-P^2) \left\{ (P^2 - 2m^2)(\omega - |\mathbf{p}|)\pi^2 T^2 \right. \\ &\quad \left. + \omega[2m^4 - P^2\{|\mathbf{p}|(\omega - |\mathbf{p}|) + m^2\}] \right\}. \end{aligned} \quad (\text{B}\cdot 3)$$

where in the third equality we have used Eqs. (A.9), (A.10) and

$$\hat{\mathbf{k}} \cdot \mathbf{q} = \frac{\mathbf{p}^2 - E_f^2 - E_b^2 + m^2}{2E_f}, \quad \hat{\mathbf{p}} \cdot \mathbf{q} = \frac{\mathbf{p}^2 - E_f^2 + E_b^2 - m^2}{2|\mathbf{p}|}. \quad (\text{B}\cdot 4)$$

For $\mathbf{p} = \mathbf{0}$, we have

$$\text{Im}\Sigma_\pm(\mathbf{0}, \omega) = -\frac{g^2}{64\pi} \omega \frac{\omega^2 + 2m^2}{m^2} \frac{(\omega^2 - m^2)^2}{\omega^4} \left(\coth \frac{\omega^2 + m^2}{4T\omega} + \tanh \frac{\omega^2 - m^2}{4T\omega} \right). \quad (\text{B}\cdot 5)$$

For the T -independent part, which is obtained by taking the $T \rightarrow 0$ limit in Eq. (B.3), we can perform the integral in Eq. (B.3) analytically, and we obtain

$$\text{Im}\Sigma_+(\mathbf{p}, \omega)_{T=0} = -\frac{g^2}{32\pi} (\omega - |\mathbf{p}|) \frac{P^2 + 2m^2}{P^2} \frac{(P^2 - m^2)^2}{P^4} \text{sgn}(\omega) \theta(P^2 - m^2), \quad (\text{B}\cdot 6)$$

with $P^2 = \omega^2 - \mathbf{p}^2$.

Appendix C

— Renormalization of the T -Independent Part —

In this appendix, we perform the renormalization of the T -independent part of the self-energy, $\Sigma(\mathbf{p}, \omega)_{T=0}$, in the models studied in §§3 and 4. Because the imaginary part of $\Sigma^R(\mathbf{p}, \omega)_{T=0}$ in both models is free from ultraviolet divergence, as shown in Appendices A and B, renormalization is needed for the real part only. The T -independent part is Lorentz covariant. To calculate $\Sigma(\mathbf{p}, \omega)_{T=0}$ by using this symmetry explicitly, we employ the self-energy in the Feynman propagator Σ^F instead of the retarded one, Σ^R . Once the renormalized self-energy in the Feynman propagator is derived, the corresponding retarded one is readily obtained. In the following, we omit the subscript of the self-energy, writing $\Sigma_{T=0}^F$ as Σ^F .

Because of the Lorentz invariance, the self-energy has the form

$$\Sigma^F(\mathbf{p}, \omega) = \not{p}\Sigma_1^F(P^2) + \Sigma_2^F(P^2), \quad (\text{C}\cdot 1)$$

with $p^\mu = (\omega, \mathbf{p})$. For the self-energy used in §3 and §4, $\Sigma_2(P^2)$ vanishes.

We regularize the real part of the self-energy by employing the subtracted dispersion relation. This is much more convenient than other regularization procedures, e.g., the Pauli-Villars and dimensional regularizations. (We have confirmed that these regularizations give the same result in our models.) The subtracted dispersion relation is written

$$\text{Re}\Sigma_1^F(P^2) = \sum_{l=0}^{n-1} \frac{(P^2 - \alpha)^l}{l!} c_l + \frac{(P^2 - \alpha)^n}{\pi} \text{P} \int_{s_{\text{thr}}}^{\infty} ds \frac{\text{Im}\Sigma_1^F(s)}{(s - P^2)(s - \alpha)^n}, \quad (\text{C}\cdot 2)$$

where α denotes the subtraction point or the renormalization point, and s_{thr} denotes the threshold, which is given by $s_{\text{thr}} = m^2$ in our case. The parameters c_l are the subtraction constants, which are to be determined by the renormalization condition. Equation (C·2) is valid for $\alpha < s$.

C.1. Renormalization in the Yukawa model with scalar coupling

From Appendix A, the imaginary part of $\Sigma_1^F(P^2)$ reads

$$\text{Im}\Sigma_1^F(P^2) = -\frac{g^2}{32\pi} \frac{(P^2 - m^2)^2}{P^4} \theta(P^2 - m^2). \quad (\text{C}\cdot 3)$$

For the real part of Σ_1^F , we use the subtracted dispersion relation given in Eq. (C·2) for $n = 1$ to regularize the ultraviolet divergence. We impose the on-shell renormalization condition, $\Sigma_1^F(P^2 = \alpha) = 0$ and $\alpha = 0$. From Eq. (C·3), we have $\text{Im}\Sigma_1^F(P^2 = 0) = 0$. The renormalized

real part is then given by

$$\begin{aligned}\text{Re}\Sigma_1^F(P^2) &= \frac{P^2}{\pi} \text{P} \int_{m^2}^{\infty} ds \frac{\text{Im}\Sigma_1^F(s)}{s(s-P^2)} \\ &= \frac{g^2}{32\pi^2} \left\{ \frac{(P^2 - m^2)^2}{P^4} \log \left| \frac{P^2 - m^2}{m^2} \right| - \frac{3}{2} + 2 \frac{m^2}{P^2} \right\}.\end{aligned}\quad (\text{C}\cdot 4)$$

The retarded self-energy, $\Sigma^R(\mathbf{p}, \omega)$, is given by $\text{Re}\Sigma^R(\mathbf{p}, \omega) = \text{Re}\Sigma^F(P^2)$ and $\text{Im}\Sigma^R(\mathbf{p}, \omega) = \epsilon(\omega)\text{Im}\Sigma^F(P^2)$:

$$\begin{aligned}\Sigma^R(\mathbf{p}, \omega) &= \frac{g^2}{32\pi^2} \not{p} \left\{ \frac{(P^2 - m^2)^2}{P^4} \log \left| \frac{P^2 - m^2}{m^2} \right| - \frac{3}{2} + 2 \frac{m^2}{P^2} \right\} \\ &\quad - i \frac{g^2}{32\pi} \not{p} \frac{(P^2 - m^2)^2}{P^4} \epsilon(\omega) \theta(P^2 - m^2).\end{aligned}\quad (\text{C}\cdot 5)$$

C.2. Renormalization in the Yukawa model with vector coupling

From Eq. (B-6), the imaginary part of the self-energy Σ_1^F reads

$$\text{Im}\Sigma_1^F(P^2) = -\frac{g^2}{32\pi} \frac{P^2 + 2m^2}{m^2} \frac{(P^2 - m^2)^2}{P^4} \theta(P^2 - m^2).\quad (\text{C}\cdot 6)$$

To renormalize the real part, we need the subtracted dispersion relation appearing in Eq. (C-2) for $n = 2$,

$$\begin{aligned}\text{Re}\Sigma_1^F(P^2) &= c_0 + c_1 P^2 + \frac{P^4}{\pi} \text{P} \int_{m^2}^{\infty} ds \frac{\text{Im}\Sigma_1^F(s)}{s^2(s-P^2)} \\ &= c_0 + c_1 P^2 \\ &\quad + \frac{g^2}{32\pi^2} \left\{ \frac{P^2 + 2m^2}{m^2} \frac{(P^2 - m^2)^2}{P^4} \log \left| \frac{P^2 - m^2}{m^2} \right| - \frac{5}{6} \frac{P^2}{m^2} - 2 + 2 \frac{m^2}{P^2} \right\},\end{aligned}\quad (\text{C}\cdot 7)$$

where we have set $\alpha = 0$. We find that the on-shell renormalization condition $\Sigma_1^F(P^2 = 0) = 0$ is not sufficient to remove all the divergent parts. Here we impose an additional condition, $c_1 = 0$, to obtain the renormalized self-energy,

$$\text{Re}\Sigma_1^F(P^2) = \frac{g^2}{32\pi^2} \left\{ \frac{P^2 + 2m^2}{m^2} \frac{(P^2 - m^2)^2}{P^4} \log \left| \frac{P^2 - m^2}{m^2} \right| - \frac{5}{6} \frac{P^2}{m^2} - 2 + 2 \frac{m^2}{P^2} \right\}.\quad (\text{C}\cdot 8)$$

Therefore, the renormalized retarded self-energy is given by

$$\begin{aligned}\Sigma_1^R(P^2) &= \frac{g^2}{32\pi^2} \left\{ \frac{P^2 + 2m^2}{m^2} \frac{(P^2 - m^2)^2}{P^4} \log \left| \frac{P^2 - m^2}{m^2} \right| - \frac{5}{6} \frac{P^2}{m^2} - 2 + 2 \frac{m^2}{P^2} \right\} \\ &\quad - i \frac{g^2}{32\pi} \frac{P^2 + 2m^2}{m^2} \frac{(P^2 - m^2)^2}{P^4} \text{sgn}(\omega) \theta(P^2 - m^2).\end{aligned}\quad (\text{C}\cdot 9)$$

Appendix D

— Limiting Behavior of $\Sigma^R(\mathbf{p}, \omega)$ in the Yukawa Model
with Vector Coupling —

In §4, we showed that the thermal mass of the quark coupled with the vector boson in the Proca formalism approaches $\omega = \sqrt{6}m$ in the high T limit, where m is the mass of the vector boson. In this section, we prove this limiting behavior. Because we are interested in the thermal mass, we only consider the quark propagator at vanishing momentum and omit the subscript and the argument of the momentum in the self-energy, writing $\Sigma_{\pm}(\mathbf{p} = 0, \omega)$ as $\Sigma(\omega)$, in the following.

Let us first derive the analytic form of $\text{Re}\Sigma(\omega)$ in the high T limit, where the T -independent part is negligible. Thus, we consider the T -dependent part $\text{Re}\Sigma(\omega)_{T \neq 0}$, which is calculated from the unsubtracted dispersion relation in Eq. (3.5),

$$\text{Re}\Sigma(\omega)_{T \neq 0} = -\frac{1}{\pi} \text{P} \int_{-\infty}^{\infty} dz \frac{\text{Im}\Sigma(z)_{T \neq 0}}{\omega - z} = -\frac{2\omega}{\pi} \text{P} \int_0^{\infty} dz \frac{\text{Im}\Sigma(z)_{T \neq 0}}{\omega^2 - z^2}. \quad (\text{D}\cdot 1)$$

In the second equality, we have used the relation $\text{Im}\Sigma(\omega) = \text{Im}\Sigma(-\omega)$, which is valid for a massless quark of vanishing momentum. Here, $\text{Im}\Sigma(\omega)_{T \neq 0}$ is given by

$$\begin{aligned} \text{Im}\Sigma(\omega)_{T \neq 0} &= -\frac{g^2}{64\pi} \frac{\omega^2 + 2m^2}{m^2} \frac{(\omega^2 - m^2)^2}{\omega^3} \\ &\quad \times \left(\coth \frac{\omega^2 + m^2}{4T\omega} + \tanh \frac{\omega^2 - m^2}{4T\omega} - 2\theta(\omega^2 - m^2) \right). \end{aligned} \quad (\text{D}\cdot 2)$$

Substituting Eq. (D.2) into Eq. (D.1), we have the following:

$$\text{Re}\Sigma(\omega)_{T \neq 0} = \frac{\omega g^2}{32\pi^2} (I_1(\omega) + I_2(\omega)), \quad (\text{D}\cdot 3)$$

$$\begin{aligned} I_1(\omega) &\equiv \text{P} \int_0^m dz \frac{1}{\omega^2 - z^2} \frac{z^2 + 2m^2}{m^2} \frac{(z^2 - m^2)^2}{z^3} \left[\coth \frac{z^2 + m^2}{4Tz} - \tanh \frac{z^2 - m^2}{4Tz} \right] \\ &= \left(\frac{T}{\omega} \right)^2 \int_0^{1/\alpha} \frac{dx}{1 - (\alpha\beta x)^2} \frac{(2 + \alpha^2 x^2)(1 - \alpha^2 x^2)^2}{x^3} \\ &\quad \times \left[\coth \left(\frac{1}{4x} + \frac{\alpha^2 x}{4} \right) - \tanh \left(\frac{1}{4x} - \frac{\alpha^2 x}{4} \right) \right], \end{aligned} \quad (\text{D}\cdot 4)$$

$$\begin{aligned} I_2(\omega) &\equiv \text{P} \int_m^{\infty} dz \frac{1}{\omega^2 - z^2} \frac{z^2 + 2m^2}{m^2} \frac{(z^2 - m^2)^2}{z^3} \left[\coth \frac{z^2 + m^2}{4Tz} - \tanh \frac{z^2 - m^2}{4Tz} - 2 \right] \\ &= -\left(\frac{T}{m} \right)^2 \int_0^{1/\alpha} \frac{dy}{1 - \alpha^2 y^2 / \beta^2} \frac{(1 + 2\alpha^2 y^2)(1 - \alpha^2 y^2)^2}{y^3} \\ &\quad \times \left[\coth \left(\frac{1}{4y} + \frac{\alpha^2 y}{4} \right) + \tanh \left(\frac{1}{4y} - \frac{\alpha^2 y}{4} \right) - 2 \right], \end{aligned} \quad (\text{D}\cdot 5)$$

with $\alpha = m/T$, $\beta = m/\omega$, $x = z/(m\alpha)$ and $y = m/(\alpha z)$.

In the high T limit ($\alpha \rightarrow 0$), the asymptotic forms of I_1 and I_2 are given by

$$\begin{aligned} I_1(\omega) &\rightarrow 2 \left(\frac{T}{\omega}\right)^2 \int_0^\infty \frac{dx}{x^3} \left[\coth\left(\frac{1}{4x}\right) - \tanh\left(\frac{1}{4x}\right) \right] \\ &= 4 \left(\frac{T}{\omega}\right)^2 \int_0^\infty dx x \left[\frac{1}{\exp(x/2) - 1} + \frac{1}{\exp(x/2) + 1} \right] \\ &= \frac{4\pi^2 T^2}{\omega^2}, \end{aligned} \tag{D-6}$$

$$\begin{aligned} I_2(\omega) &\rightarrow - \left(\frac{T}{m}\right)^2 \int_0^\infty \frac{dy}{y^3} \left[\coth\left(\frac{1}{4y}\right) + \tanh\left(\frac{1}{4y}\right) - 2 \right] \\ &= -2 \left(\frac{T}{m}\right)^2 \int_0^\infty dy y \left[\frac{1}{\exp(y/2) - 1} - \frac{1}{\exp(y/2) + 1} \right] \\ &= -\frac{2\pi^2 T^2}{3m^2}. \end{aligned} \tag{D-7}$$

We have confirmed that the correction terms due to the finite value of α are $O(\alpha \ln(1/\alpha))$. Therefore, the self-energy in the high T limit is given by

$$\lim_{T \rightarrow 0} \text{Re}\Sigma(\omega) = \frac{g^2 T^2}{8} \left(\frac{1}{\omega} - \frac{\omega}{6m^2} \right). \tag{D-8}$$

In this case, the quasi-dispersion relation is given by the solution of the equation $\omega - \text{Re}\Sigma(\omega) \approx -\text{Re}\Sigma(\omega) = 0$, i.e., the zero of $\text{Re}\Sigma(\omega)$. Therefore, in this model, the energy $\omega = \sqrt{6}m$ gives the thermal mass in the high T limit.

References

- 1) I. Arsene et al. (BRAHMS Collaboration), Nucl. Phys. A **757** (2005), 1.
 B. B. Back et al. (PHOBOS Collaboration), Nucl. Phys. A **757** (2005), 28.
 J. Adams et al. (STAR Collaboration), Nucl. Phys. A **757** (2005), 102.
 K. Adcox et al. (PHENIX Collaboration), Nucl. Phys. A **757** (2005), 184.
- 2) T. Umeda, R. Katayama, O. Miyamura and H. Matsufuru, Int. J. Mod. Phys. A **16** (2001), 2215.
 M. Asakawa and T. Hatsuda, Phys. Rev. Lett. **92** (2004), 012001.
 S. Datta, F. Karsch, P. Petreczky and I. Wetzorke, Phys. Rev. D **69** (2004), 094507.
 T. Umeda, K. Nomura and H. Matsufuru, Eur. Phys. J. C **39S1** (2005), 9.
- 3) T. Matsui and H. Satz, Phys. Lett. B **178** (1986), 416.
- 4) T. Hatsuda and T. Kunihiro, Phys. Lett. B **145** (1984), 7.
- 5) C. DeTar, Phys. Rev. D **32** (1985), 276.

- 6) R. J. Fries, B. Müller, C. Nonaka and S. A. Bass, Phys. Rev. Lett. **90** (2003), 202303; Phys. Rev. C **68** (2003), 044902.
V. Greco, C. M. Ko and P. Levai, Phys. Rev. Lett. **90** (2003), 202302.
S. A. Voloshin, Nucl. Phys. A **715** (2003), 379.
D. Molnar and S. A. Voloshin, Phys. Rev. Lett. **91** (2003), 092301.
- 7) M. Kitazawa, T. Kunihiro and Y. Nemoto, Phys. Lett. B **633** (2006), 269; see also hep-ph/0510381.
- 8) M. Asakawa, S. A. Bass and B. Müller, Prog. Theor. Phys. **116** (2006), 725.
- 9) R. D. Pisarski, Phys. Rev. Lett. **63** (1989), 1129.
E. Braaten and R. D. Pisarski, Nucl. Phys. B **337** (1990), 569; *ibid.* **339** (1990), 310.
J. Frenkel and J. C. Taylor, Nucl. Phys. B **334** (1990), 199.
- 10) See for example, M. Le Bellac, *Thermal Field Theory* (Cambridge University Press, Cambridge, England, 1996).
- 11) V. P. Silin, Sov. Phys. JETP **11** (1960), 1136.
- 12) H. A. Weldon, Phys. Rev. D **26** (1982), 1394.
- 13) V. V. Klimov, Sov. J. Nucl. Phys. **33** (1981), 934; Yadern. Fiz. **33** (1981), 1734.
- 14) H. A. Weldon, Phys. Rev. D **40** (1989), 2410; Physica A **158** (1989), 169; Phys. Rev. D **61** (2000), 036003.
- 15) J. P. Blaizot and J. Y. Ollitrault, Phys. Rev. D **48** (1993), 1390.
- 16) M. Kitazawa, T. Koide, T. Kunihiro and Y. Nemoto, Phys. Rev. D **70** (2004), 056003.
- 17) M. Kitazawa, T. Koide, T. Kunihiro and Y. Nemoto, Prog. Theor. Phys. **114** (2005), 205.
- 18) M. Kitazawa, T. Koide, T. Kunihiro and Y. Nemoto, Phys. Rev. D **65** (2002), 091504.
- 19) M. Kitazawa, T. Kunihiro and Y. Nemoto, Phys. Lett. B **631** (2005), 157.
- 20) B. Janko, J. Mary and K. Levin, Phys. Rev. B **56** (1997), R11407.
- 21) G. Baym, J. P. Blaizot and B. Svetitsky, Phys. Rev. D **46** (1992), 4043.
- 22) H. A. Weldon, Phys. Rev. D **28** (1983), 2007.
- 23) A. Peshier, K. Schertler and M. H. Thoma, Ann. of Phys. **266** (1998), 162.
- 24) See for example, C. Itzykson and J.B. Zuber, *Quantum Field Theory* (McGraw-Hill, New York, 1980).
T. Cheng and L. Li, *Gauge theory of elementary particle physics* (Oxford University Press, New York, 1984).
- 25) E. V. Shuryak and I. Zahed, Phys. Rev. C **70** (2004), 021901; Phys. Rev. D **70** (2004), 054507.
- 26) G. E. Brown, C. H. Lee, M. Rho and E. Shuryak, Nucl. Phys. A **740** (2004), 171; J. of Phys. G **30** (2004), S1275.

- H. J. Park, C. H. Lee and G. E. Brown, Nucl. Phys. A **763** (2005), 197.
G. E. Brown, B. A. Gelman and M. Rho, Phys. Rev. Lett. **96** (2006), 132301.
G. E. Brown, C. H. Lee and M. Rho, nucl-th/0507011.
- 27) E. Braaten, R. D. Pisarski and T. C. Yuan, Phys. Rev. Lett. **64** (1990), 2242.
28) Y. Yanase, Y. Jujo, T. Nomura, H. Ikeda, T. Hotta and K. Yamada, Phys. Rep. **387** (2003), 1.
29) D. Boyanovsky, Phys. Rev. D **72** (2005), 033004.
30) K. Mitsutani, M. Kitazawa, T. Kunihiro and Y. Nemoto, in progress.
31) M. Kitazawa, T. Kunihiro and Y. Nemoto, in progress.